STRUCTRAL AND FUNCTIONAL CONSEQUENCES OF A SINUS TACHYCARDIA-ASSOCIATED MUTATION ON THE REGULATION OF PACEMAKER CHANNEL BY CYCLIC NUCLEOTIDES

by

JOANNA XIA

BSc. (Honours), The University of British Columbia, 2018

A THESIS SUBMITTED IN PARTIAL FULFILLMENT OF THE REQUIREMENTS FOR THE DEGREE OF

MASTER OF SCIENCE

in

THE FACULTY OF GRADUATE AND POSTDOCTORAL STUDIES

(Cell and Developmental Biology)

THE UNIVERSITY OF BRITISH COLUMBIA
(Vancouver)

June 2022

The following individuals certify that they have read, and recommend to the Faculty of Graduate and Postdoctoral Studies for acceptance, the thesis entitled:

Structural and functional consequences of a sinus tachycardia-associated mutation on the regulation of pacemaker channel by cyclic nucleotides

Submitted by Joanna Xia in partial fulfillment of the requirements for

the degree of Master of Science

in Cell and Developmental Biology

Examining Committee:

Eric Accili, Associate Professor, Cellular and Physiological Sciences, UBC

Supervisor

Vanessa Auld, Professor, Zoology, UBC

Supervisory Committee Member

Filip Van Petegem, Professor, Biochemistry and Molecular Biology, UBC

Supervisory Committee Member

Edwin Moore, Professor, Cellular and Physiological Sciences, UBC

Additional Examiner

Abstract

The "funny" (I_f) current, which is generated by HCN (Hyperpolarization-activated cyclic nucleotide-gated channels), contributes to the diastolic depolarization phase of the action potential. Regulation of I_f by cAMP represents a key mechanism by which heart rate is autonomically regulated. HCN channels open more easily when cyclic nucleotides (cAMP or cGMP) bind to a domain in the intracellular C-terminus in each of the four identical subunits. Disease-associated mutations in HCN often interfere with the regulation of HCN by cAMP. Therefore, understanding how the cAMP regulation is perturbed in the context of diseases is the first step to developing targeted therapies and treatment. Here, we analyze the effect of the first discovered gain-of-function mutation, R524Q, in HCN isoform 4. This mutation is found in a region called the C-linker that connects the cyclic nucleotide-binding domain to the pore. Previously published concentration-response curves collected from electrophysiology experiments show that R524Q results in increased cAMP potency, as seen from a shift of the concentration-response relation to lower levels of cAMP. However, it is unclear whether it can be attributed to the effect on cyclic nucleotide binding affinity or the impact on downstream structural change and channel gating. We used isothermal titration calorimetry to determine the binding of cAMP to a naturally occurring tetramer of the C-linker and CNBD of the HCN4 channel. For both the mutant and wild type, we found that cAMP bound to the protein with negative cooperativity, and the high and low binding affinities for cAMP were not significantly different between WT and mutant. We also reported a crystal structure of the HCN4 C-terminus carrying the R524Q mutation. The mutation did not cause significant change to the global structure. However, it impacts a salt bridge with the transmembrane S4-S5 domain which plays an important role in keeping channel closed. Our results suggest the shift of the concentration-

response relation in HCN4 R524Q mutant may be largely attributed to processes downstream that couple cAMP binding to channel opening.

Lay Summary

We all have a group of cells in the pacemaker channel of our heart that control our heart rate. During exercise, our heart rate increases because adrenaline in the body produces a special signaling molecule, called cAMP, that binds to the pacemaker protein. My research proposal focuses on a mutation in the pacemaker protein, that is found in patients with Inappropriate Sinus Tachycardia (IST). Patients with IST have an abnormally fast resting heart rate which heavily limits the amount of allowed physical activities. Since the mutation has been found to amplify the effect of cAMP on the pacemaker channel, my research proposal seeks to understand how the pacemaker channel responds to cAMP differently because of the mutation, through structural and binding analysis. The results of our studies will further knowledge of the mutation's role in IST and improve understanding of how we can develop targeted drug therapies.

Preface

This thesis is an original intellectual product of the author, Joanna Xia, under the supervision of Dr. Eric Accili at the University of British Columbia.

I was responsible for designing and performing experiments, as well as data analysis and figures preparation. The thesis contains work that is in preparation for publication in a peer-reviewed journal. F. Van Petegem provided guidance in solving the mutant crystal structure and in developing the experiment. E. Accili was the supervisory author and oversaw the entire project.

Dynamic Light Scattering (Chapter 2.5) was done in collaboration with Dr. Anson Chan at Murphy Lab at UBC, with the details being outlined in the methods section.

Table of Contents

List of Tables

List of Figures

List of Abbreviations

ACh	Acetylcholine
βME	beta-mercaptoethanol
cAMP	adenosine-3',5'-cyclic monophosphate
cCMP	cytidine-3', 5'-cyclic monophosphate
cGMP	guanosine-3', 5'-cyclic monophosphate
CCP4	collaborative computational project number 4
CNBD	cyclic nucleotide binding domain
Coot	crystallographic object-oriented toolkit
ΔG	Gibb's free energy
ΔH	enthalpy
ΔS	entropy
DLS	Dynamic light scattering
EC_{50}	Half maximal effective concentration ($K_{1/2}$)
HCN	hyperpolarization-activated cyclic nucleotide-gated (channel)
HMT	His_6-MBP-TEV protease cleavage site (tag)
ITC	Isothermal Titration Calorimetry
I_f	Funny current
PIP_2	Phosphatidylinositol-4,5-biphosphate
PKA	Protein Kinase A
SA node	Sinoatrial node
TEV	tobacco etch virus
TRIP8b	Tetratricopeptide-repeat-containing Rab8b-interacting protein
TM	transmembrane
$V_{1/2}$	Mid-point voltage of activation fitted by Boltzmann function
V_{max}	maximal voltage shift at saturating cNMP concentrations
VSD	Voltage-sensing domain
ZMW	Zero-mode waveguides

Acknowledgements

I would like to start by expressing my sincere gratitude to Dr. Eric Accili, for giving me the opportunity to conduct my MSc. thesis in his lab. I'm grateful for his guidance and mentorship, and for his kindness and generosity. I'm also thankful for my committee members, Dr. Vanessa Auld and Dr. Filip Van Petegem for their constructive advice. In addition, I'm very appreciative of the opportunity to learn X-ray crystallography from Dr. Filip Van Petegem through taking his course and through his mentorship.

I would also like to expression my appreciation for some of the past and current members in Accili Lab and Van Petegem Lab. Drs. Zhuren Wang and Maitree Biswas helped me get oriented at the initial stages of MSc. and created an inclusive and intellectually stimulating work environment. Drs. Sarah Chow and Leo Ng were the first two people in the lab who conducted ITC measurements on isolated HCN CNBD domains and provided a solid foundation for the ensuing work (and my thesis). I'm indebted to the mentorship of Drs. Ciaran Mcfarlane and Omid Haji-Ghassemi as their incredible teaching enabled me to conduct protein purification, ITC, and crystallography independently.

I'm also thankful for the friendship and companionship of my colleagues. Britany, getting to know you is a major highlight of my grad school experience. Thank you for being a great friend, brunch buddy, coffee date, and fellow violin enthusiast all in one.

Last but not least, I'm grateful for the unconditional love and support from my family. Mom and dad, thank you for always being encouraging of my endeavours to pursue further education and for believing in my potential. I look up to your hard work, tenacity, and creativity - they are a major source of inspiration for me whenever I encounter any obstacles.

Dedication

To my parent

Chapter 1: Introduction

1.1 Introduction of the sinoatrial node and funny current (I_f)

Maintaining a heart rate that would sustain physiological demands is critical for ensuring good health. In mammals heart rate is dictated by the duration of the diastolic depolarization of sinoatrial node (SAN node) cells which is mainly determined by the pacemaker I_f current (Baruscotti *et al.*, 2010). Located at the junction of the superior vena cava and the right atria, the SAN is a collection of heterogeneous cells, including pacemaker cells as well as non-pacemaker cells such as atrial myocytes, adipocytes and fibroblasts (Boyett *et al.*, 2000). SAN is the primary site where the normal heartbeat is initiated. A defining characteristic of cells in the pacemaker is their automaticity, an ability to generate an action potential without an external stimulus (Baruscotti *et al.*, 2005; Barbuti *et al.*, 2007; DiFrancesco, 2010). These cells generate the funny current (I_f) which is an inward current activated on hyperpolarization to the diastolic range of voltage (Baruscotti *et al.*, 2005; Barbuti *et al.*, 2007; DiFrancesco, 2010). The contribution of I_f to the diastolic depolarization potential is essential for the activation of Ca^{2+} channels which result in the activation potential spike. Therefore, the I_f is a major player in generating spontaneous activity and controlling the frequency of action potential firing, which dictates heart rate (Baruscotti *et al.*, 2005; Barbuti *et al.*, 2007; DiFrancesco, 2010).

Upon initial discovery, the funny current was known as I_{K2}. The current was initially thought to be a pure potassium current because of its properties, such as having a recorded reversal potential that varies with the external K concentration (Hauswirth *et al.*, 1968). To distinguish from the very fast-activating or instantaneous potassium current called I_{K1}, this newly discovered slowly-activating current in Purkinje fibres was called I_{K2}. Adrenaline was thought to steepen the slope of diastolic depolarization by decreasing the contribution of I_{K2} ((Kassebaum &

Van Dyke, 1966; Hauswirth *et al.*, 1968). The properties of I_{K2} were further elucidated after the current was re-analyzed in Purkinje fibres and compared with the funny current of the sinoatrial node (Brown *et al.*, 1979; DiFrancesco & Ojeda, 1980; Yanagihara & Irisawa, 1980; DiFrancesco, 1981). It was found that I_K contributes less to the diastolic depolarization than the slow inward current I_f. Both I_{K2} of Purkinje fibres and funny current of the SA node were found to have different properties compared to a pure potassium current, including activation by hyperpolarization from approximately -40mV, a mixed current with both sodium and potassium, and inhibition by cesium but not barium (Yanagihara & Irisawa, 1980; DiFrancesco, 1981). In the SAN, I_f has a threshold of activation around -40/-45mV whereas in Purkinje fibres, the current is activated at more negative voltages, corresponding to a more negative voltage range of diastolic depolarization (Figure 1.1) (DiFrancesco *et al.*, 1986; DiFrancesco, 1993)

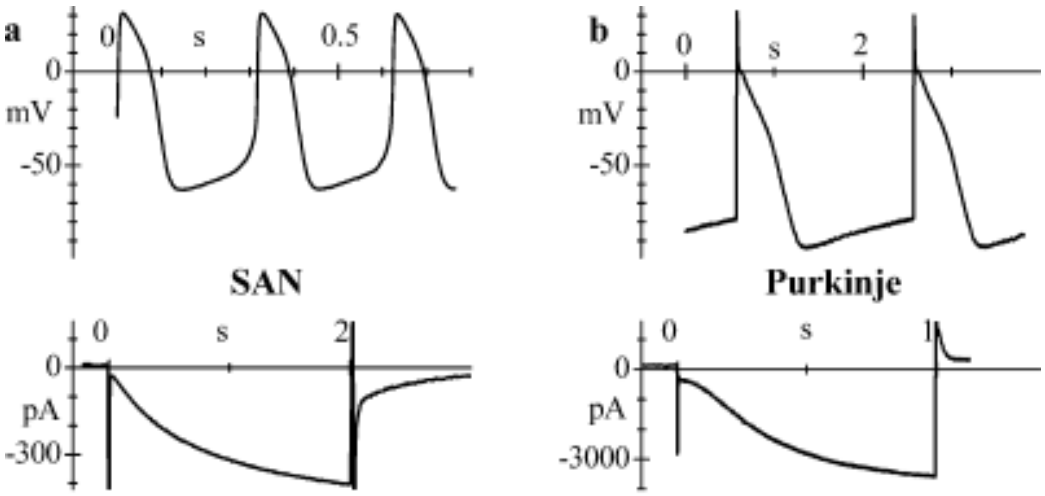

Figure 1.1. Sample action potentials (upper) and I_f current records (lower) in a SAN cell (a) and in a Purkinje fibre (b)
In the SAN, I_f has a threshold of activation around -40/-45 mV while in Purkinje fibres, the current is activated at more negative voltages and therefore has a more negative voltage range of diastolic depolarization. The ability for I_f to activate at negative voltages is essential for action potential firing because it allows membrane potential to become sufficiently positive for Ca^{2+} channels to open (adapted from Barbuti *et al.,*2007, with permission)

1.2 Hyperpolarization-activated Cyclic Nucleotide-gated (HCN) channels underlie the funny current

1.2.1 Unique biophysical properties of HCN

HCN channels belong to the superfamily of six-transmembrane segment channels and are related to cyclic nucleotide-gated (CNG) channels and voltage-dependent K^+ (K_v) channels K_v10-K_v12. HCN channels have several unique biophysical properties that distinguish them from other members of the family. First, despite containing the essential amino acids in their selectivity filter that confer K^+ selectivity, HCN permits K^+ by Na^+ by a ratio of ~4:1 which is significantly lower than the selectivity of K^+ channels which select K^+ over Na^+ by a ratio of greater than 1000:1 (Yellen, 1984; Neyton & Miller, 1988; Gauss *et al.*, 1998; Ludwig *et al.*,

1998; Santoro *et al.*, 1998). The permeability of HCN to both K^+ and Na^+ result in a reversal potential of -20 to -30 mV under physiological conditions. Therefore, the opening of HCN channels allow an influx of cations which cause depolarization and raise the membrane potential to be sufficiently positive to allow L-type calcium channels to open. Second, unlike many other voltage-dependent ion channels where depolarization causes opening, HCN has a reversed polarity, opening upon hyperpolarizing and closing upon depolarization. Finally, cyclic nucleotides, in particular cyclic AMP and cGMP increase the opening probability of HCN channels, but they are not a prerequisite for channel opening as in CNG channels (Lee & MacKinnon, 2017).

The pore of HCN channel is initially closed as the voltage sensor adopts a depolarized conformation. The S4 helix is unusually long and contains two additional helical turns on the cytoplasmic side compared with other voltage-dependent channels. This allows it to extend into the cytoplasm, contact the C-linker and twist the gate shut. Upon hyperpolarization, the voltage-driven displacement of S4 is thought to destabilize the interactions that previously held the pore closed, thereby allowing the S6 helices to spontaneously open (Lee & MacKinnon, 2019). Binding of cAMP induces small local conformational changes, in particular the C-linker rotation and S6 helix displacement that biases the channel towards the direction of pore opening (Lee & MacKinnon, 2017).

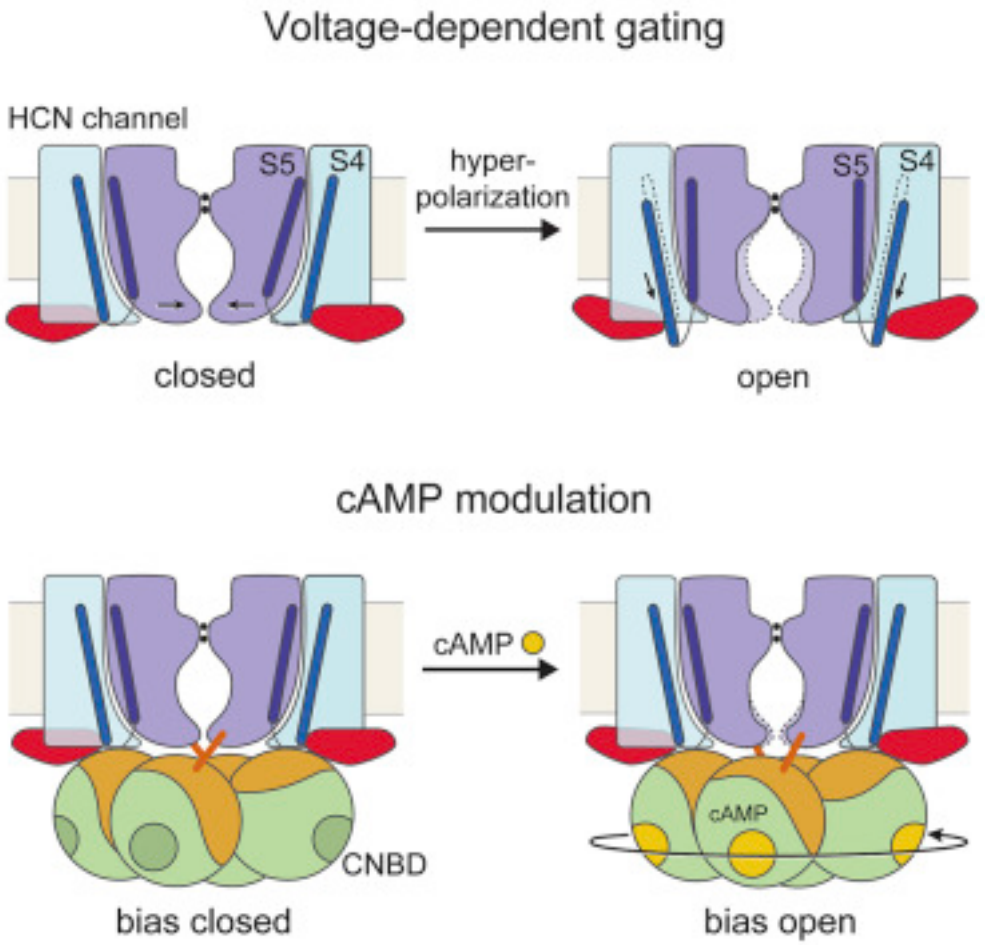

Figure 1.2 Schematic of HCN voltage-dependent gating and cAMP modulation of HCN gating

The pore is initially closed as the voltage sensor adopts a depolarized conformation. The length of S4 helix allows it to extend into the cytoplasm, contact the C-linker and twist the inner gate shut. Upon membrane hyperpolarization, the voltage-driven downward displacement of the S4 helix will disrupt the interactions that initially stabilized the closing pore, allowing the S6 helices to spontaneously open. Binding of cAMP induces local conformational changes that are spread to other parts of the channel. These changes rotate the gate-forming inner helices which bias the channel towards an open conformation (Adapted from (Lee & MacKinnon, 2017) with permission).

1.2.2 Expression and distribution of HCN isoforms

Hyperpolarization-activated cyclic nucleotide-gated (HCN) channels underlie the funny current. HCN has 4 isoforms, HCN1-4 which differ in their expression in the body and are

expressed most prominently expressed in the heart and nervous system. In the sinoatrial node (SAN), HCN4 is the predominant isoform expressed, although there is evidence for lower levels of expression for HCN1 and HCN2 (Ishii *et al.*, 1999; Shi *et al.*, 1999; Moroni *et al.*, 2001; Whitaker *et al.*, 2007). HCN1, HCN4 and HCN2 are also selectively expressed in different areas of the bundle branches. HCN4 is the only isoform that is expressed in the atrioventricular bundle, while HCN1 and HCN2 represent the dominant atrial and ventricular isoform, respectively(Herrmann *et al.*, 2011). All HCN isoforms are expressed in the mammalian brain(Robinson & Siegelbaum, 2003). HCN1 and HCN2 are the major isoforms expressed in both the central nervous system (CNS) and peripheral nervous system (PNS). HCN1 and HCN2 are expressed in the dorsal root ganglion (DRG) in the PNS (Brewster *et al.*, 2007; Seo *et al.*, 2015). Both isoforms are also expressed in the cerebral cortex, cerebellar cortex, basal ganglia, and hippocampus of PNS (Brewster *et al.*, 2007; Seo *et al.*, 2015). HCN3 shows the weakest expression in the brain and heart compared to the other three isoforms (Robinson & Siegelbaum, 2003).

1.2.3 Crystal and cryo-EM structures of HCN isoforms

The general topology of HCN family is present in all the four HCN isoforms. Key canonical sequence features include six (S1-S6) conserved transmembrane segments with the voltage sensor and pore domain, as well as a C-terminal systolic domain which includes the C-linker and the cyclic nucleotide binding domain (CNBD) (Figure 1.3).

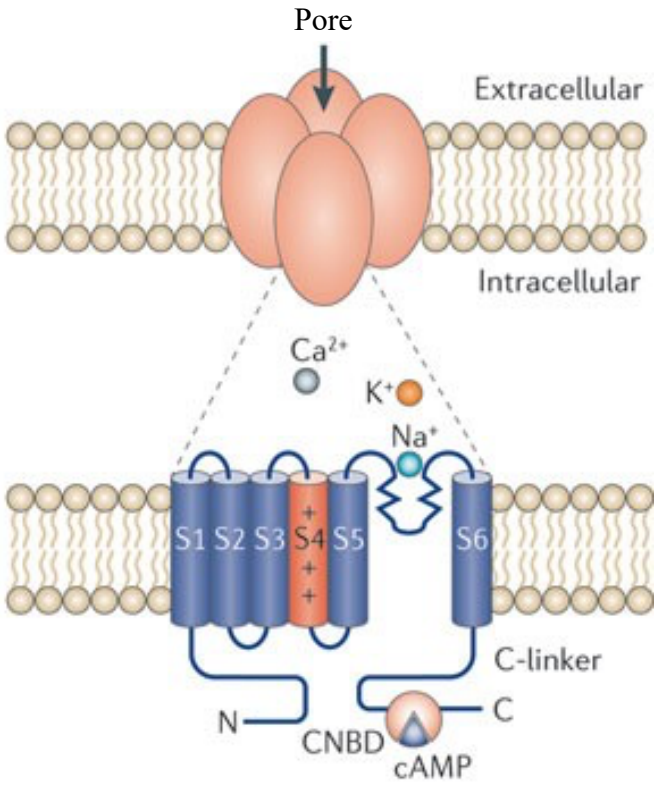

Figure 1.3 Schematic topology of HCN channels.
The fours HCN isoforms (HCN1-4) share a general topology including 6 transmembrane domains (S1-S6). S1-S4 are the voltage sensor domains whereas S5-S5 are the pore domains. The S6 is connected to the carboxyl-terminal region which consists of the C-linker domain and the cyclic nucleotide-binding domain (CNBD) (adapted from Postea & Biel, 2011, with permission)

The full-length structure of HCN1 was solved in 2017, which gives insight into the structural basis underlying the reversed polarity of HCN channels (Lee & MacKinnon, 2017). The voltage sensor of HCN channels differs from that of other voltage-dependent channels in that it is longer and contains two additional helical turns on the cytoplasmic side. The extended S4 brings S4-S5 linker in contact with the C-linker of a neighboring subunit, which keeps the gate in a closed conformation under depolarized conditions. Structural features, including the packing arrangement of S4, S5 and S6 helices and the HCN domain, are thought to stabilize the

closed pore in the context of a depolarized voltage sensor. Hyperpolarization drives the displacement of S4 helix through charge interactions, relieving the constraints that S4 place on the C-linker and S6 and disrupting the stabilizing interactions, therefore allowing the pore to open.

The recently solved cryo-EM structure of HCN4 (Saponaro *et al.*, 2021), in combination with the published crystal structure of HCN4 CL-CNBD (Xu *et al.*, 2010), further advanced our understanding of cyclic AMP regulation of HCN4 on a structural level. While the cAMP-bound (holo) structure of HCN4 is overall similar in 3D Structure to cAMP-bound HCN1, local structural differences were observed in the S4-S5 linker and in the C-linker region (Figure 1.4). Significantly, the S4-S5 linker of one subunit forms a contact with the underlying C-linker (B' helix) of another subunit, which is made possible by the helical conformation of the S4-S5 linker in HCN4. This contact enabled a tetrad to form between the transmembrane domain and the C-linker. This tetrad was found to only be present in cAMP-bound form and was postulated to act as a Mg^{2+} coordination site that is essential to the cAMP-dependent regulation of HCN4. This contact is not present in HCN1 due to the different conformation of S4-S5 linker (Figure 1.4).

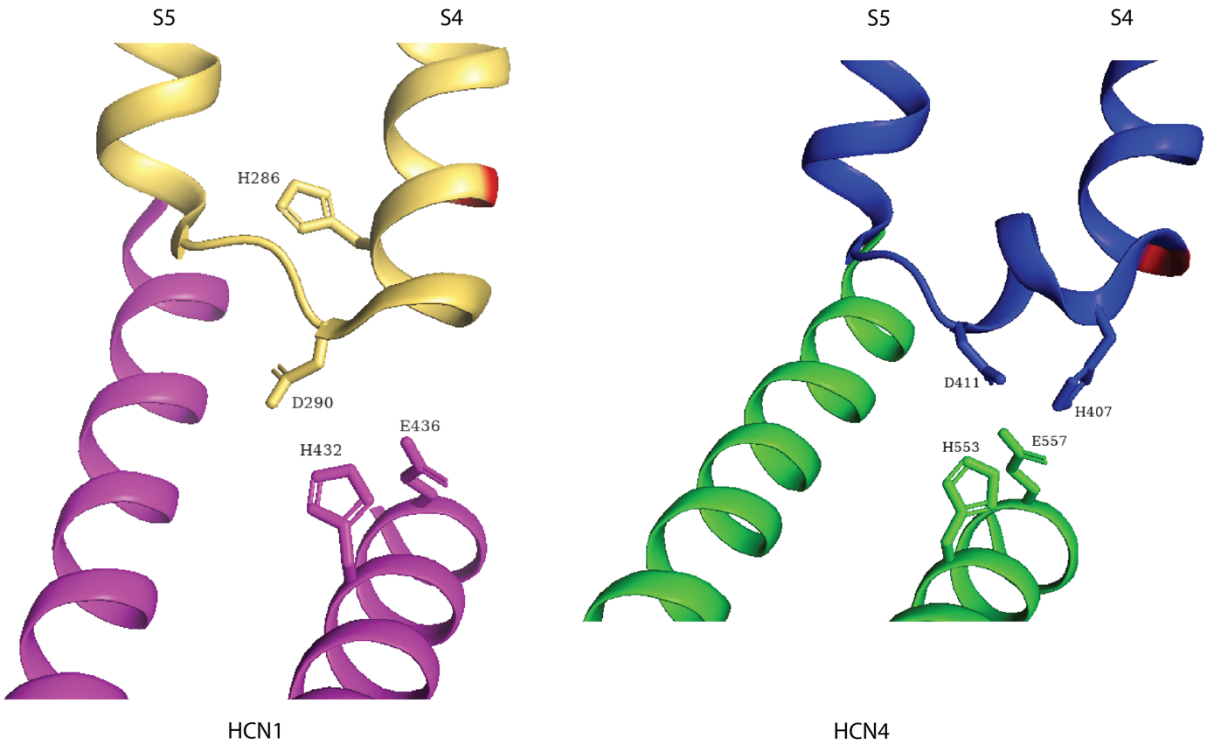

Figure 1.4 Comparison of the tetrad region of HCN4 with the corresponding region in HCN1
The helical turn of S4 in HCN4 (right) due to the I405 backbone structure (shown in red) results in the formation of a tetrad between two residues (H407, D411) in the S4-S5 linker and two residues (H553, E557) in the B' helix of the C-linker region. The equivalent of I405 in HCN1 is I284 which adopts a different conformation. As a result, the equivalent HCN4 "tetrad" residues in HCN1 do not form a triad (equivalent residues shown as sticks)

In addition, the structure of the C-terminus (C-linker and CNBD) of HCN1, HCN2 and HCN4 were solved by X-ray crystallography in the presence of cAMP (Zagotta *et al.*, 2003; Xu *et al.*, 2010; Lolicato *et al.*, 2011). The construct used in the crystallography starts right at the end of the S6 transmembrane segment and extends through the C-linker and CNBD. This is also the same region of HCN4 that is used for experiments in this thesis. The C-linker is comprised of six α-helices (A'-F'), followed by the CNBD which includes four $\propto$-helices (A,P,B,C). A β-roll resides between the A- and B- helices and consists of eight β-strands. Cyclic AMP and cyclic

GMP bind in the anti and syn configuration, respectively, inside the β-roll and interact with β-roll and C-helix. The C-linker and CNBD in the four subunits form a four-fold symmetric gating, with the C-linkers playing a critical part in mediating the intersubunit interactions. In the solved structure (Zagotta *et al.*, 2003), cAMP binds in the anti-configuration while cGMP binds in the syn configuration in the cyclic nucleotide binding pocket.

In addition, the solved crystal structures for various HCN isoforms have elucidated the differences in the interactions formed by cAMP and cGMP with β-roll and C-helix in the cyclic CNBD region of HCN, which accounts at least partially for the nucleotide specificity and the higher concentration of cGMP required to produce an effect. The role of close contacts in the HCN channel and CNG channel that contribute to ligand (cAMP and cGMP) specificity has been examined using information from the solved structures, molecular dynamics simulations and patch clamp electrophysiology (Flynn *et al.*, 2007; Zhou & Siegelbaum, 2007). These studies have shown that a residue in the C-helix (R632 in HCN2) is crucial for the efficacy of cAMP and cGMP. In addition, certain residues (e.g. Thr 592 in HCN2) confers cGMP sensitivity, whereas certain residues in the C-helix (R635, I636 and K638) provide the energetic contribution to preferentially stabilize cAMP, conferring the overall greater sensitivity of HCN channels for cAMP over cGMP. While these residues are mainly located in the CNBD region, mutations far away from the CNBD region, including the R524Q mutation that is investigated in this thesis, also has an impact on cAMP sensitivity. Through structural studies and binding affinity measurements, we aim to elucidate some of the factors that contribute to changes in cAMP sensitivity upon a single residue mutation.

1.3. Impact of cyclic nucleotides on the funny current (If)

1.3.1 Early discovery of the effect of cyclic AMP and cyclic GMP on funny current

Brown et al. found that applying adrenaline to the sinoatrial node increases the heart rate by increasing the slope of diastolic depolarization, and this is due to an increase in the inward current (Brown *et al.*, 1979). The effect of adrenaline is thought to be mediated by the beta-adrenergic receptor because it is mimicked by isoprenaline (DiFrancesco *et al.*, 1986). Acetylcholine has the opposite effect of adrenaline on the funny current, which is thought to be mediated by the muscarinic receptor (DiFrancesco & Tromba, 1988). The increase in funny current (I_f) by adrenaline is associated with an increase in cyclic AMP production, whereas the decrease in I_f by acetylcholine is associated with a decrease in cAMP production. However, how cyclic AMP exerts its action on the funny channel was initially unclear. Studies on calcium and potassium channels found that cyclic AMP acted through the cAMP-dependent protein kinase A, which regulates channel activity by phosphorylation (Osterrieder *et al.*, 1982; Shuster *et al.*, 1985). It was unknown whether the cAMP regulates funny current in the sinoatrial node also through channel phosphorylation. To investigate this, DiFrancesco and Tortora performed excised patch experiments on cardiac pacemaker cells. They showed that directly applying PKA to the cytoplasmic side had no effect on I_f (DiFrancesco & Tortora, 1991). The addition of cyclic AMP results in a depolarizing shift in the shift of channel activation range, which ranges from ~11 to 14 mV in the SAN (DiFrancesco & Tortora, 1991; DiFrancesco & Mangoni, 1994). It also accounts for most of the combined effect of acetylcholine and isoprenaline on the funny current in individual pacemaker cells, which is approximately 18mV (Accili *et al.*, 1997). Both adrenaline and cAMP also have a similar effect of decreasing the first latency of individual channel opening at given voltages and shifting the activation curve to less-negative voltages

(DiFrancesco, 1986; DiFrancesco & Mangoni, 1994). Therefore, these results provide evidence that the effect of adrenaline on the funny current is mediated by cAMP, in a PKA-independent manner.

DiFrancesco and Tortora also analyzed the direct effect of cGMP (Figure 1.5). A saturating concentration of cyclic GMP produces a similar shift in voltage as cyclic AMP. However, the potency of cyclic GMP (as indicated by the EC50 value) is about 30 times lower than that of cyclic AMP. Although the potency is lower, cGMP does have an impact on the activation curve at a concentration lower than $1\mu M$. This indicates that cGMP may have an impact on the funny channel of the heart under physiological or pathophysiological conditions. However, the lower potency of cGMP compared to cAMP implies that the effect of cGMP may only become significant when cAMP levels are low or when cGMP accumulates to significant levels in areas of the heart where funny channels are located. This leads us to question whether a mutation that impacts cAMP potency would also affect the response of the channel to cGMP, which is investigated in the context of R524Q mutation in HCN4 in this thesis.

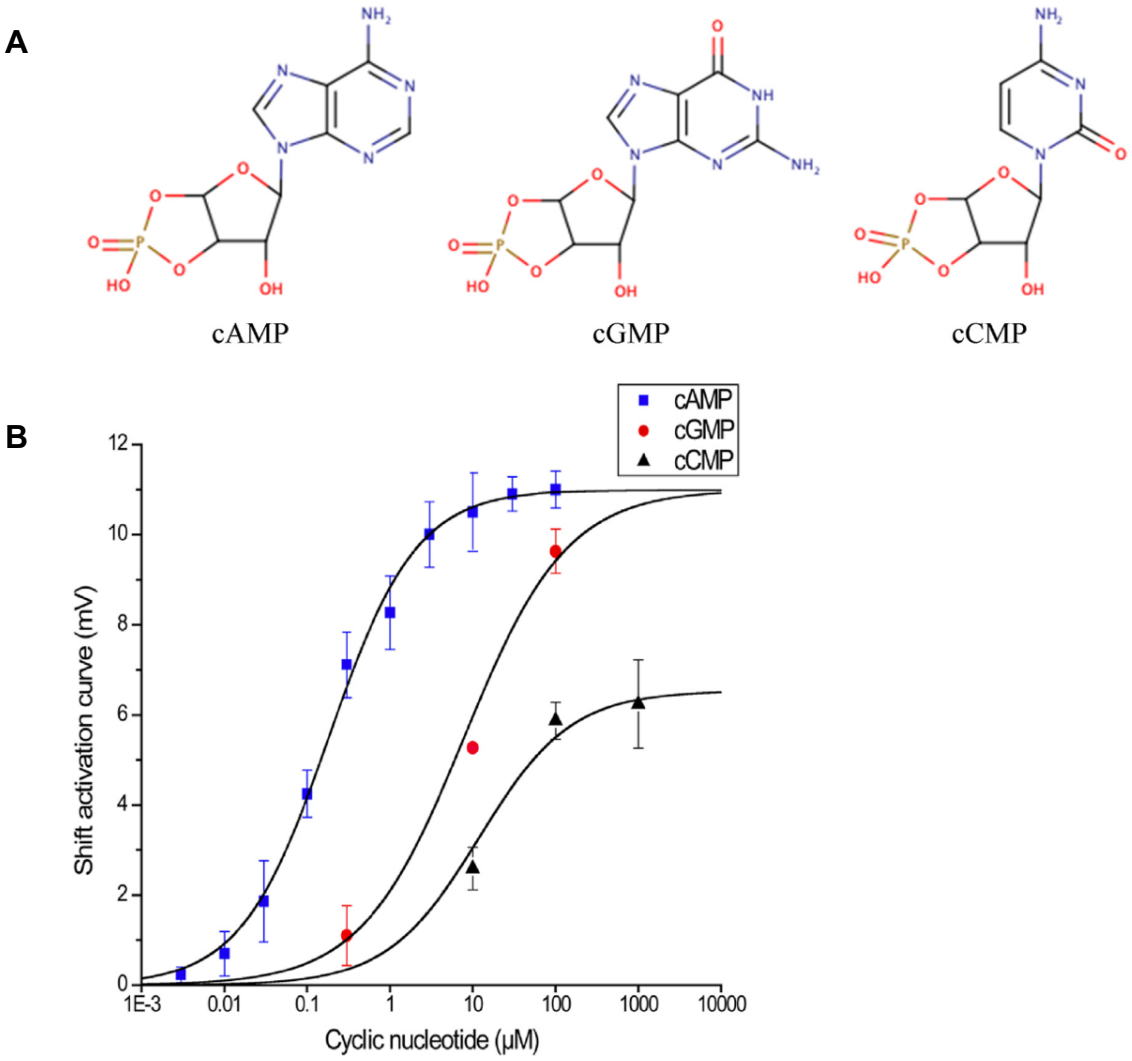

Figure 1.5 (A) Structure of the three ligands. (B) Concentration-response relationship for the shift of If activation curve as a function of cyclic nucleotide concentration.
I_f channels from the membrane of isolated rabbit sino-atrial node myocytes were used for the I_f activation curve, and the concentration-response curve was generated by measuring cAMP-induced shifts of the I_f activation curve for different cAMP concentrations. The data points for cAMP were reproduced using GetDataGraph Digitizer, and the original data for cGMP and cCMP specified in DiFrancesco and Tortora (1991). Fitting was performed using the Hill function in Origin 7.

1.3.2 Facilitation of channel opening by cAMP in different HCN isoforms

Different HCN isoforms have similar biophysical qualities but differ quantitively in their properties. HCN1 has a faster activation and deactivation kinetics compared to HCN2 and HCN4, and the activation threshold of HCN2 is more negative than that of HCN1 or HCN4 (Altomare *et al.*, 2001; Moosmang *et al.*, 2001). Different HCN isoforms are impacted to a variable extent by the binding of cAMP, and the difference in cAMP modulation is partially due to the interaction between the CNBD and other intracellular regions such as the C-linker (Ludwig *et al.*, 1999; Seifert *et al.*, 1999; Viscomi *et al.*, 2001; Wang *et al.*, 2001; Elinder *et al.*, 2006). HCN2 and HCN4 are modulated to a greater extent by cAMP compared to HCN1. Cyclic AMP results in a shift of +15 to +25 mV for HCN2 and HCN4 isoforms, but only a shift in the range of +2 to +7 mV for HCN1 (Ludwig *et al.*, 1999; Seifert *et al.*, 1999; Viscomi *et al.*, 2001; Wang *et al.*, 2001; Elinder *et al.*, 2006) (Figure 1.6). Human HCN3 channels, on the other hand, do not have a positive shift in the activation curve in response to cAMP (Stieber *et al.*, 2005).

The HCN2 isoform is the most studied of all known vertebrate and invertebrate isoforms. It was shown, using this isoform, that the C-linker and CNBD are primarily responsible for the effect of cAMP on the activation curve (Wainger *et al.*, 2001). Cyclic AMP relieves the inhibition of these connected domains on the opening of the channel. Differences in the extent of cAMP modulation between the HCN1 and HCN2 isoforms result largely from the greater auto-inhibitory effect of CNBD in HCN2 (Wainger *et al.*, 2001). The ITC binding experiments in our lab revealed no evidence for a high affinity binding transition in HCN1, which supports a theory that HCN1 is "preactivated" and would explain a less negative basal $V_{1/2}$ compared to other HCN isoforms.

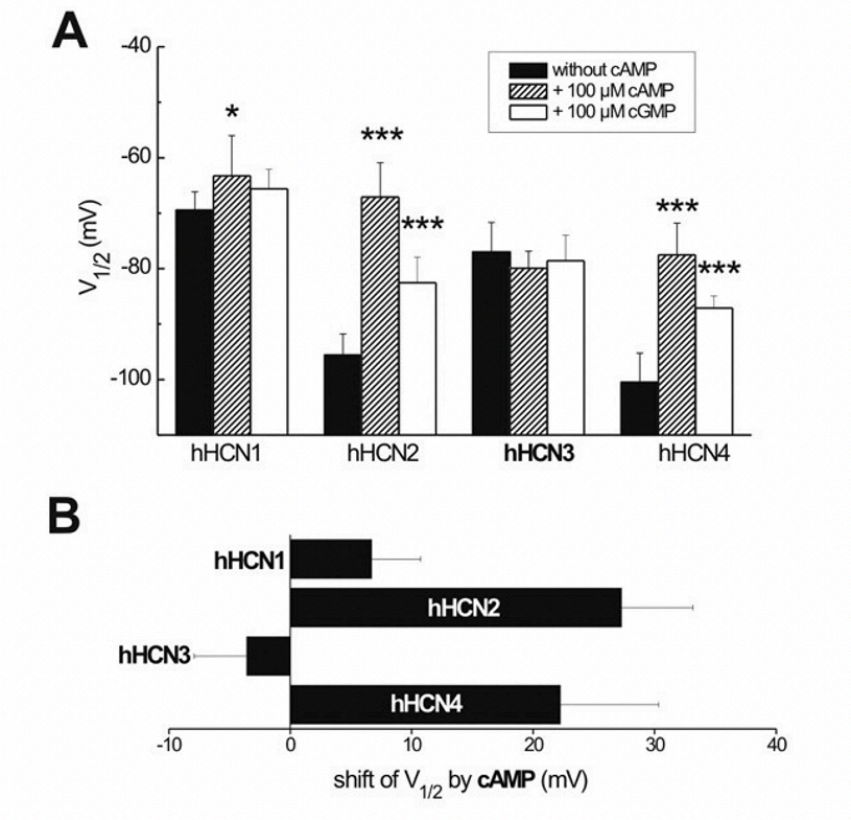

Figure 1.6 cAMP modulation of the four HCN isoforms expressed in HEK cells
Human HCN channels were expressed in HEK293 cells to generate stable cell lines, where electrophysiological properties of the four isoforms were measured. (A) The half-activation voltage shows the difference in basal $V_{1/2}$ between the four isoforms. HCN1 and HCN3 have less negative $V_{1/2}$ and are proposed to be pre-activated. $V_{1/2}$ of all HCN channels after application of 100μM 8-Br-cAMP (cAMP analog) or 100μM pCPT-cGMP (cGMP analog) were also shown in comparison. ***$p<0.0001$, *$p<0.05$ (B) Difference in the shift of $V_{1/2}$ upon addition of cAMP in the four isoforms. Adapted from (Stieber et al., 2005) with permission.

1.4 Negative cooperativity of HCN2 and HCN4 in their direct binding to cAMP

Determining the binding affinities of cyclic nucleotides is important for discerning the basis behind the differential response of HCN to cyclic nucleotides (as evidenced by difference in shift of $V_{1/2}$) as a result of single-point mutations in HCN isoforms. In order to directly measure the binding affinities of cyclic nucleotides on the channel, previous PhD students in

Accili lab, Dr. Sarah Chow and Dr. Leo Ng, developed an approach using Isothermal Titration Calorimetry to directly measure the binding of cAMP to the tetrameric C-terminus of the HCN2 channel (Chow *et al.*, 2012b; Ng *et al.*, 2016). This region is important because binding of cAMP to the C-terminus of HCN relieves the auto-inhibitory effect of CNBD on the transmembrane domain, which facilitates channel opening. Isolating this region of the HCN2, which consists of C-linker and CNBD, allows measurement of direct binding affinity without the impact of transmembrane domains. Adding cAMP to 200μM of purified HCN2 protein produced two clear transitions by ITC, which could readily be fit with a two independent binding site model. Both a high affinity binding value of 0.12μM and a low-affinity binding value of 1.5 μM were calculated from the model fitting. The stoichiometry associated with high binding affinity was in an approximate ratio of 1:3 to the stoichiometry associated with the low binding affinity, suggesting that cAMP binds to one subunit with high affinity and binds to the other 3 subunits with low affinity. ITC binding experiments on both HCN2 and HCN4 suggest that these two isoforms display negative cooperativity in cAMP binding at high protein concentrations. HCN1, however, displays no evidence for a high affinity binding transition, despite having a similar low affinity binding value compared to HCN2 and HCN4. The data suggest that changes induced by the high affinity binding of cAMP have already occurred in the HCN1 C-terminus even in the absence of cAMP. This "preactivation" of HCN1 is thought to contribute to the smaller effect of cAMP on facilitation of channel opening the more positive activation curve in the absence of cAMP (Altomare *et al.*, 2001; Wainger *et al.*, 2001; Wang *et al.*, 2001). The results suggest that the negative cooperativity observed in HCN2 and HCN4 may be the result of initial binding of cAMP to the unoccupied tetramers that change the conformation of the other subunits, so that the binding of cAMP to the remaining three subunits becomes less favorable.

In addition Kusch et al. (2011) measured the binding of fcAMP, a fluorescent derivative of cAMP, in the full-length HCN2 and also found that cAMP binds with negative cooperativity (Kusch *et al.*, 2011). Kusch et al. demonstrated a more complex cooperativity, where the binding of second cAMP was found to be more favorable than the binding of first cAMP, whereas the binding of third cAMP was found to be unfavourable and the fourth cAMP favourable, demonstrating a "positive-negative-positive" cooperativity. Nevertheless, the results from the Accili lab and those from Kusch et al. were similar in that more than one binding affinity was involved, and a pronounced negative cooperativity effect for ligand binding was observed in both these studies. This is somewhat surprising given the four-fold symmetry of HCN2 C-linker/CNBD observed in structural studies.

The binding energetics of cAMP to the HCN2 C-terminal tetramer suggest that the initial high affinity binding event is associated with favourable entropy and enthalpy whereas low affinity binding to the second subunit occurs with favourable enthalpy but unfavourable entropy. The entropy-driven negative cooperativity aligns with studies of another cAMP-binding protein, the catabolite-activating proteins (CAP) (Popovych *et al.*, 2006). CAP forms a dimer to which cAMP also binds with negative cooperativity, and the thermodynamic basis for the observed negative cooperativity was proposed to be entirely entropic based on a comparison of ΔH and ΔS in high-affinity and low-affinity binding events.

Variations in experimental methods also contribute to the discrepancies in the observed cooperativity of pacemaker channels. A recently published paper used nanophotonic zero-mode waveguides (ZMWs) to monitor the individual ligand binding event to multimeric HCN1 and HCN2 ion channels (White *et al.*, 2021) Their results showed that cAMP binds independently to all four subunits when the pore is closed, in the absence of membrane potential. Differences in

experimental methods could partially account for the observed differences in cooperativity status. The most significant differences are using a full-length channel in a closed conformation (White *et al.*, 2021) versus using isolated CNBD (Chow *et al.*, 2012a), and measuring cAMP binding to high concentrations of protein with ITC experiments (White *et al.*, 2021) versus measuring fcAMP binding to individual, immobilized HCN1/HCN2 using ZMWs (White *et al.*, 2021). However, despite the difference in observed cooperativity, the K_a values are similar between ZMW measurement (HCN1SM and HCN2 SM in Figure 1.7) and ITC measurement (HCN1J cAMP and HCN2J cAMP in Figure 1.7). These results suggest that it may be possible that the measuring cAMP binding affinity for the isolated CNBD, the experimental approach utilized in this thesis, would generate a similar result as measuring the binding affinity to full-length HCN channels using an alternative approach (e.g. ZMW).

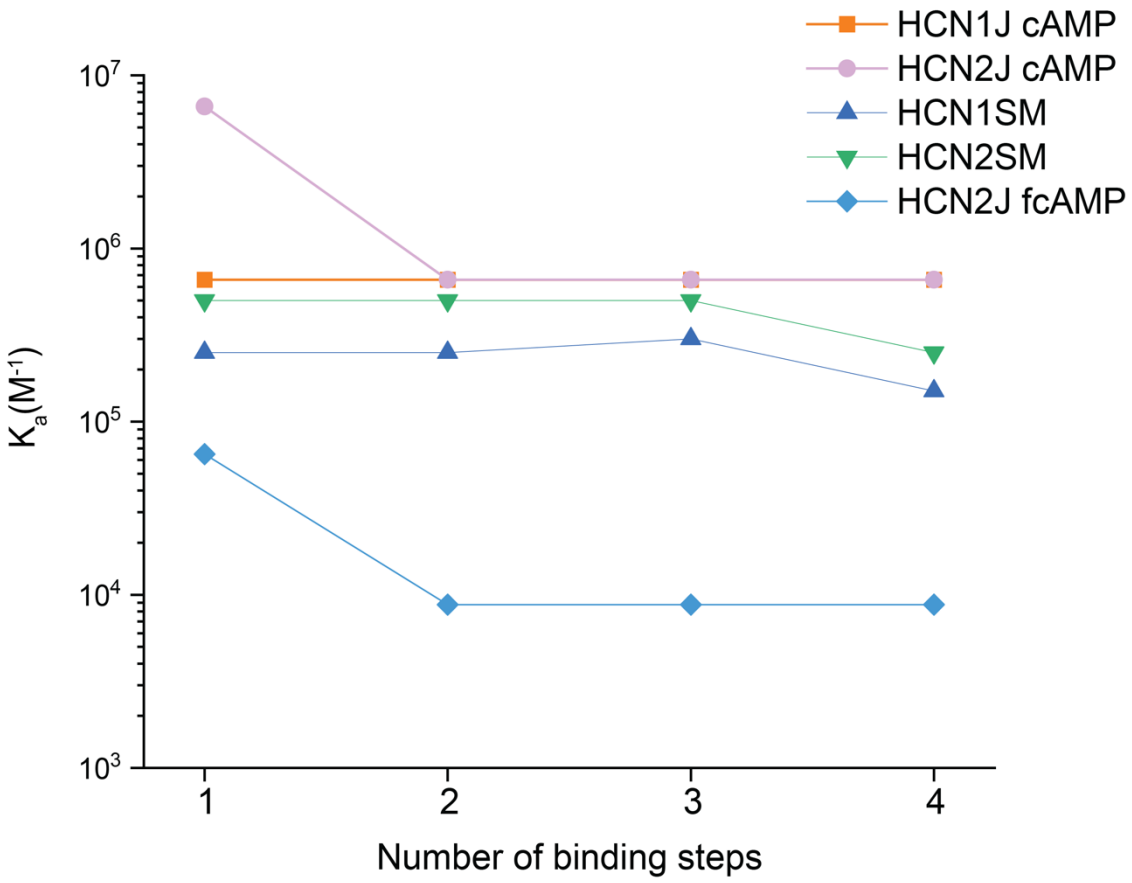

Figure 1.7 Equilibrium association constants (K_a) for each ligand-binding step measured from different experimental methods

HCN1J and HCN2J refer to the C-terminus region (C-linker and CNBD) of HCN1 and HCN2 respectively, used for purification and ITC binding measurements in the Accili Lab. HCN1J cAMP and HCN2J cAMP represent K_a values obtained from ITC measurements, which measured the binding of cAMP to HCN1J and HCN2J respectively. Methods were described in detail in Chow *et al.,* 2012a. HCN2J fcAMP represent K_a values also obtained from ITC measurements but using fcAMP (a fluorescent cAMP anaolog) as the ligand as a more direct comparison to data from the Chanda Lab. HCN1SM and HCN2SM are full-length HCN1 and HCN2 channels used in the Chanda Lab. Binding experiments using fcAMP were conducted by depositing full-length HCN molecules into nanophotonic zero-mode waveguides, with methods detailed in White *et al.,* 2021.

1.5 Disease-associated mutations in HCN4

The SA node acts as the natural pacemaker of the heart because of its ability to spontaneously generate an electrical impulse, which then travels to the rest of the heart's electrical conduction system (Easterling *et al.*, 2021). Disruptions of the SA node may result in a failure of the sinus node to create a heart rate that meets the body's needs. The sick sinus syndrome has been defined as the "intrinsic inadequacy of the sinoatrial node (SAN) to perform its pacemaking function due to a disorder of automaticity and/or inability to transmit its impulse to the rest of the atrium (Bigger & Reiffel, 1979). In 2003, familial sick sinus syndrome was found to be associated with mutations in the HCN gene family that mediates I_f in the heart(Schulze-Bahr *et al.*, 2003). Both HCN1-deficient (Fenske *et al.*, 2013) and HCN2-deficient (Ludwig *et al.*, 2003) transgenic mice may display a sick sinus syndrome phenotype. However, among the 4 HCN isoforms, mutations that affect I_f in the human heart have only been discovered in HCN4 gene (Schulze-Bahr *et al.*, 2003; Ueda *et al.*, 2004; Milanesi *et al.*, 2006; Nof *et al.*, 2007; Laish-Farkash *et al.*, 2010; Schweizer *et al.*, 2010; Duhme *et al.*, 2013; Macri *et al.*, 2014; Milano *et al.*, 2014; Schweizer *et al.*, 2014; Zhou *et al.*, 2014). The structural or functional effects of these mutations and their associated pathophysiology were well summarized in Verkerk and Wilders, 2015 and are shown in figure 1.7. The C-linker/CNBD domain harbour most of the disease-associated mutations in HCN4. Some of these mutations are also located at the N-terminus, S4-S5 linker region and in the selectivity filter between transmembrane domains S5 and S6.

1.5.1 HCN4 mutations in the pore region and in S4-S5 linker

Mutations located in the pore region include G480, Y481H, G482R and A485V. G480, a point mutation in the HCN4 cardiac ion channel pore, is found in a family with asymptomatic

sinus bradycardia (Nof *et al.*, 2007). The mutation shifts the activation curve to more negative voltages. As well, protein expression is reduced in the mutant channel, affecting trafficking of the channel to the membrane. A485V is located just outside the selectivity filter and is associated with symptomatic sinus bradycardia in Moroccan Jews (Laish-Farkash *et al.*, 2010). The mutation results in a hyperpolarizing shift of activation curve and decreased protein synthesis. Y481H and G482R are located in the selectivity filter between the transmembrane domains S5 and S6. These two mutations are found in multiple families with a combined clinical presentation of bradycardia and LVNC (left ventricular noncompaction cardiomyopathy) (Milano *et al.*, 2014). These two mutations also shift the voltage dependence of activation to more negative potentials. A414G is the mutation described in the S4-S5 linker. It also results in a hyperpolarizing shift in the voltage dependence of activation. All the above-mentioned mutations which result in a negative shift in the activation curve would result in lower current density in the potential range of diastolic depolarization.

1.5.2 HCN4 mutations that result in C-terminus truncation

Two of the disease-associated mutations in the C-linker/CNBD region of HCN4 truncate the CNBD region. L573X mutation, a mutation which leaves HCN4 without a CNBD domain, is found in a patient with an idiopathic sinus node disease (Schulze-Bahr *et al.*, 2003). This mutation does not disrupt intracellular trafficking or I_f current in the absence of cAMP. However, this mutation makes the protein unresponsive to increases in intracellular cAMP concentration, and changes activation and deactivation kinetics. E617X is another mutation that results in a C-terminally truncated HCN4 and is associated with sinus bradycardia. Similar to L573X, the mutation also results in a lack of response to cAMP, as indicated by a lack of positive shift in the activation curve in the presence of cAMP (Schweizer *et al.*, 2010).

1.5.3 Other disease-associated mutations in the C-linker/CNBD of HCN4

In addition to L573X, the truncation mutation, K530 and D553N are the other two disease-associated mutations in the C-linker region of HCN4. The K530N mutation is found in patients with tachycardia-bradycardia and persistent atrial fibrillation (Duhme *et al.*, 2013). The homomeric mutant HCN4-K530N channels do not differ in their activation curves compared to HCN4 WT. However, in heteromeric channels, there is significant hyperpolarizing shift of the half-maximal activation voltage, which likely results from the impaired interaction between neighbouring mutant and wild-type subunits. Reaction to cAMP is not impaired in the heteromeric or homomeric mutant channels. The D553N mutation is found in a patient who suffers from cardiac syncope that is a result of severe bradycardia, prolonged QT interval and polymorphic ventricular tachycardia. Decreased current density is observed in mutant, which is possibly due to a trafficking defect (Ueda *et al.*, 2004). The S672R mutation is located in the CNBD region and is associated with familial sinus bradycardia (Milanesi *et al.*, 2006). The mutation slows current deactivation and shifts the activation curve to hyperpolarized voltages in the absence and presence of endogenous cAMP. In addition, submicromolar concentrations of cAMP causes a smaller shift in the activation curve in the S672R mutant compared to the WT. However, comparing the dose-response curves of WT and S672 mutant channels, similar potency (or $K_{1/2}$) values were obtained in integral HCN4 channels (Milanesi *et al.*, 2006). The crystal structure of S672 mutant C-terminus (C-linker/CNBD) has been solved and reveals no significant global changes in the structure, except a disordered loop on the cAMP entry path (Xu *et al.*, 2012).

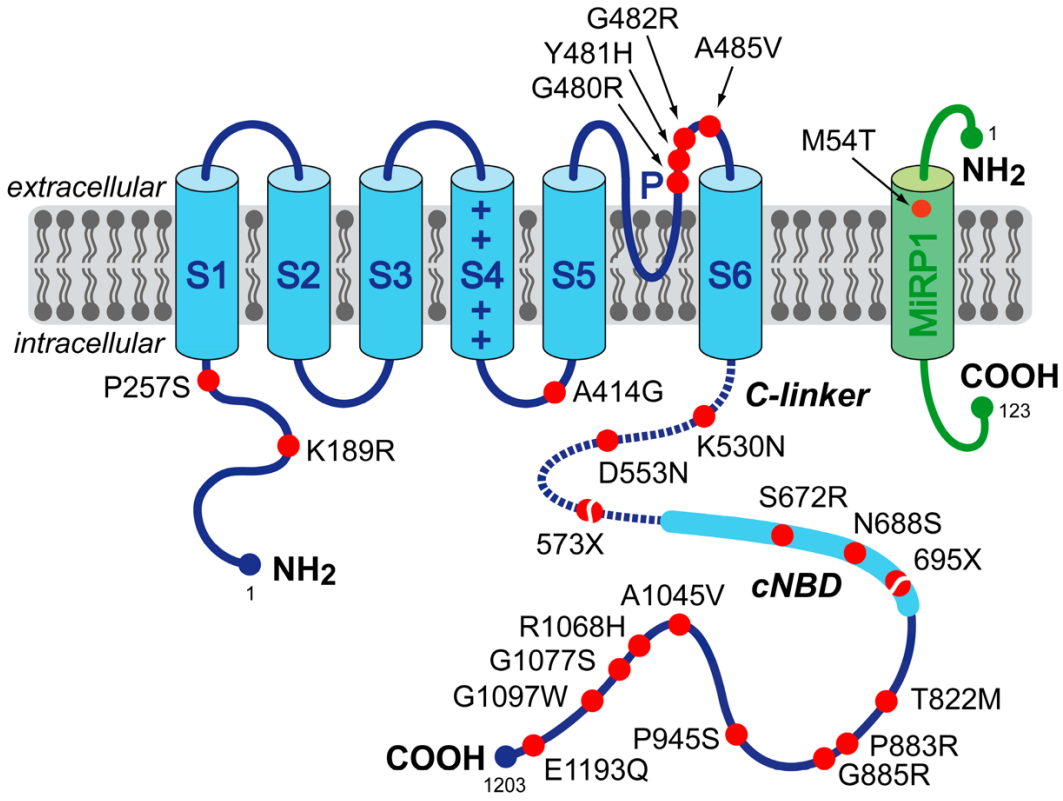

Figure 1.8 Schematic topology of the HCN4 protein and locations of known mutations in the HCN4 protein (adapted from Verker and Wilders, 2015, with permission)
Red dots indicate the HCN4 mutation sites that are associated with clinical established or potential sinus node dysfunction that have been discovered so far. The split dots represent the truncations resulting from 573X and 695X truncating mutations.

1.6 A newly discovered gain-of-function mutation in HCN4

While most of the uncovered mutations in human HCN4 channels lead to loss-of-function and are associated with bradycardia, the arginine-to-glutamine mutation (R524Q) is the first discovered gain-of-function mutation in HCN4 and is found in patients with Inappropriate Sinus Tachycardia (IST) (Baruscotti *et al.*, 2017). Patients with IST have a higher resting heart rate than expected, which cannot be explained by physiological demands or conditions known commonly to increase heart rate, and heavily limits the amount of allowed physical activities in these patients (Baruscotti *et al.*, 2017; Olshansky & Sullivan, 2019). Figure 1.9 (top) shows the

ECG of a patient diagnosed with inappropriate sinus tachycardia while the bottom of the figure shows the ECG of the same patient after they recovered. The R524Q mutation is in the initial part of the C-linker, a region that connects the S6 transmembrane domain to the cyclic nucleotide binding domain (Figure 1.10). The association of this mutation with increased pacemaker channel activity was confirmed by evidence that when spontaneously beating rat newborn myocytes were transfected with R524Q mutant HCN4 channels, they exhibited a faster rate compared to when transfected with wild-type HCN4 channels. Through patch clamp experiments, researchers addressed the question of whether the changes of the activation curve in the mutant is due to a difference in intrinsic channel property or a difference in the sensitivity of HCN channels to basal cytoplasmic cAMP level (Baruscotti *et al.*, 2017). Using inside-out macropatch experiments with both a physiological and saturating concentration of cAMP, Baruscotti et al. demonstrated the difference between activation curves for wild-type and R524Q mutant with due to the difference in sensitivity to cAMP. Concentration-response curves of cAMP dependence of activation curve shift was measured in inside-out micropatches and showed that R524Q results in increased cAMP potency (Figure 1.11). While the maximal shift at saturating cAMP concentration was similar for wt, wt-R524Q, and R524Q channels, at around 11.9mV, the K_d value is lower for WT-R524Q (0.35μM) and R524Q channels (0.080μM) compared to WT channels (1.67 μM) (Figure 1.11). This means that it takes a lower concentration of cAMP to have the same effect on R524Q mutant compared to the WT channels, which is a physiologically important difference when cAMP is lower than the saturating level in the SA node.

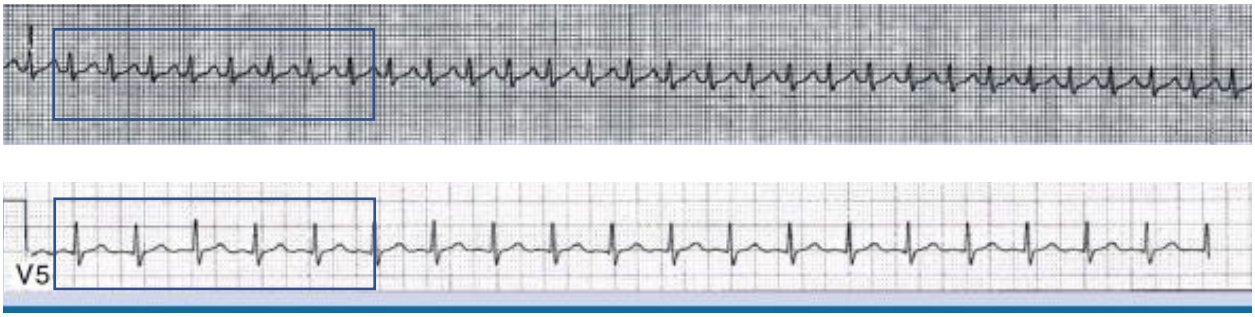

Figure 1.9 ECG comparison of a patient with Inappropriate Sinus Tachycardia (top) and ECG of the same patient after their recovery from IST (bottom)

Patients with Inappropriate Sinus Tachycardia have higher sinus rate than usual (usually above 100 beats/min) that cannot be explained by normal physiologic demands. The abnormally high sinus rate is associated with symptoms such as palpitation, dizziness and syncope after minimal amount of physical activity. The high sinus rate also makes P-wave morphology difficult to characterize. Upon recovery from IST (bottom) P-wave morphology becomes much more distinguishable.

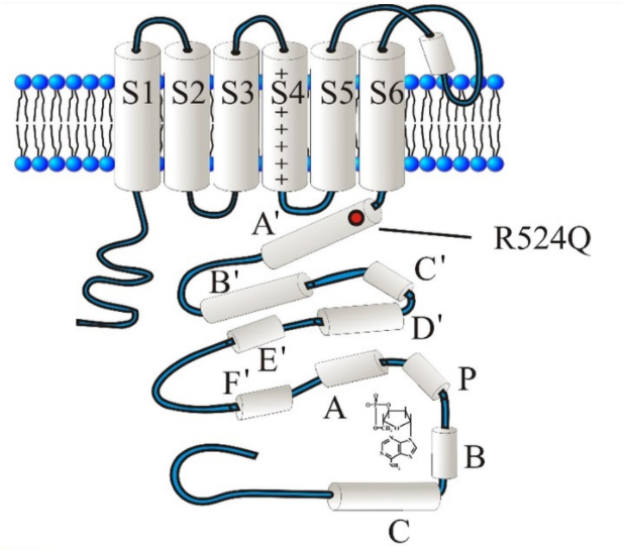

Figure 1.10 Topology of one HCN4 channel subunit showing the spatial localization of the R524Q mutation

The six transmembrane domains (S1-S6) and the intracellular N- and C-terminus are shown. The C-linker includes six α-helices and the cyclic nucleotide-binding domain includes 4 α-helices (A,P,B and C) as indicated. The red dot indicates the approximate position of the mutation R524Q (Adapted from (Baruscotti *et al.*, 2017) with permission).

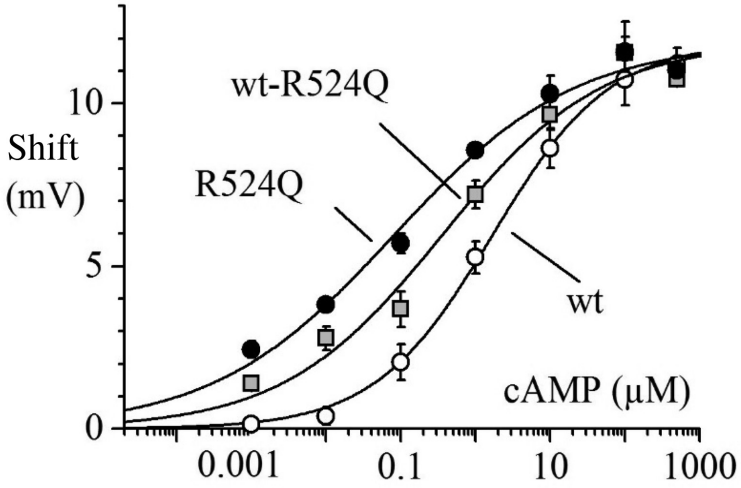

Figure 1.11 Dose-response relationships of activation curve shift (shift in $V_{1/2}$) in varying cAMP concentrations.

Measurements were done in inside-out macropatches expressing wt, wt-R524Q, and R524Q channels, respectively. Each datapoint is the average of 4-10 exposures. Parameters of Hill fitting of these curves are: K_d=1.67, 0.35, and 0.080μM and h=0.55, 0.41, and 0.36 for wt, wt-R524Q, and R524Q channels, respectively. Maximal shift was fixed to 11.9mV for all curves (adapted from Baruscotti et al., 2015 with permission).

1.7 Thesis question and hypothesis

The binding of cAMP results in several downstream effects: a change in the local conformation of CNBD, propagation of the pore through C-linker, which results in the functional impact of cAMP to facilitate voltage-dependent gating. The purpose of this thesis is primarily to investigate whether the larger response of the R524Q mutant channel to lower concentrations of cAMP is a result of altered cyclic nucleotide binding or changes in subsequent conformation or gating. To address the above question, we have examined cyclic nucleotide binding to a naturally occurring tetrameric form of the wild type and R524Q HCN4 C-terminal region. Comparing and contrasting the binding affinities of cyclic AMP and cyclic GMP to WT and mutant could give us insight into whether the mutation alters direct cAMP binding, or downstream gating, or a combination of both. We also addressed the structural basis of the effects of R524Q mutation by solving a crystal structure of the mutant C-terminus bound to cAMP. My hypothesis is since the mutation is far away from the C-linker/CNBD region, the binding affinities will not change due to the R524Q mutation, but rather the shift of the concentration response curve to lower concentrations of cAMP is due to alterations in downstream gating as a result of the mutation.

Chapter 2 Experimental Methods

2.1 Site-directed mutagenesis and protein expression

The rabbit HCN4 C-linker/CNBD template was amplified and inserted into a modified pET28 vector. In the inserted vector, an HMT tag (containing a His-tag, maltose binding protein, and TEV cleavage site) was introduced before the C-linker/CNBD of interest with an HMT (His-tag, maltose binding protein, and TEV cleavage site) inserted in the N-terminal side of the construct. The cloning was completed by Dr. Sarah Chow, a previous PhD student in the lab (Chow *et al.*, 2012a). Refer to **Appendix 1A** for a schematic diagram of the protein. His-tag enables protein to bind to talon column during affinity chromatography, maltose-binding protein ensures solubility of proteins and the cleavage site is specific to TEV protease, which cleaves the tag from the protein of interest.

The R524Q single point mutation was made using site-directed mutagenesis following the Quikchange protocol (Strategene). Refer to **Appendix 2A** for the sets of primers to flank the mutation site. After the PCR program, DpnI restriction enzyme was used to treat the reaction product to digest the methylated template DNA at 37℃ overnight. The digested products were transformed in DH5∝ E. coli cells and plated for colonies.

Cells were cultured in LB media (10g/L biotryptone, 10g/L yeast extract and 5g/L sodium chloride) with antibiotics (kanamycin and chloramphenicol) at 37℃, shaking at 210rpm for 3-4 hours. When optical density (OD) reached the range of 0.6-0.8, protein synthesis was induced by 0.1M IPTG. Cells were grown at 25℃ for 17hr (overnight) before harvesting. The cell pellets were frozen at -60℃ before centrifugation. A glycerol stock (600μL of culture at OD0.6 and 400μL of filtered glycerol) was prepared for future protein induction and expression.

2.2 Protein purification

Protein purification was performed as described previously (Chow *et al.*, 2012a, b; Ng *et al.*, 2016; Ng *et al.*, 2019). Harvested cells were resolubilized in 40mL lysis buffer containing buffer A (250mM KCl, 10mM Hepes, pH 7.4), 5% glycerol, 375μM EDTA, 25μg/ml DNase I, 1mM PMSF and lysozyme. The mixture is lysed by sonication for 12min (1sec pulse on, 2sec pulse off) and centrifuged for 30min at 35,000xg to remove cell debris. The filtered supernatant was loaded onto a cobalt affinity column (Talon, Clontech) where the His-tagged protein would bind to the talon column. The column is then washed with buffer A and eluted with buffer B (250mM KCl, 500mM imidazole, pH 7.4) so that the His-tagged protein of interest gets eluted and separated out from other proteins. The HMT tag was cleaved by TEV protease (Accili Laboratory) inside a 3.5 kDa dialysis membrane containing 80μL of 0.5M EDTA and 1:1000βME and the dialysis was done in 2L of buffer A and 10mM βME overnight. The cleaved products were subject to Talon column again where the HMT tag would get trapped in the column and C-linker/CNBD was in the flow-through. An extra column volume of 6% imidazole was used to allow complete elution. Lastly, the C-linker/CNBD was purified by a cationic exchanger (ResourceS, GE Healthcare). The protein was first charged by dialyzing in a low-salt buffer for 3hr, and later eluted with an increasing [KCl] gradient up to 1M KCl, at 4℃. SDS Gel was run to confirm and collect the protein of interest and collected protein was dialyzed in "ITC buffer" (150mM KCl, 10mM Hepes, pH 7.4) overnight. Proteins were concentrated to 200μM for ITC and to 500μM for X-ray crystallography. Purity was confirmed with SDS, and concentration was measured by spectrophotometry with Edelhoch (6M guanidine hydrochloride (Fisher Scientific; 50-01-1), 20mM $NaPO_4$ (Bioshop Canada; 10049-21-5), pH6.6) to dilute and denature the protein.

2.3 Ligand preparation

Cyclic AMP and cyclic GMP were obtained in powder form from Sigma. Ligands were dissolved in ITC buffer to make a stock of 10mM or 20mM.

2.4 Isothermal Titration Calorimetry

Isothermal Titration Calorimetry (ITC) was carried out at 25°C in the ITC200 instrument (Malvern). Cyclic AMP or cGMP was titrated into the sample cell containing 200μM of respective purified protein constructs. They were titrated either 1μl at a time for a total of 40 injections or titrated 2 μl at a time for a total of 20 injections. The reference cell is filled with filtered water. Water, instead of ITC buffer was used for the reference cell for cleaning purposes, and because it has been shown that filling the reference with water sufficiently balances the heat capacity of the sample cell and that instrument response is similar whether buffer or water is in the reference cell. At least 3 replicates from 2 protein purification trials were conducted for each protein-ligand combination. Upon each injection, the heat difference between the sample and reference cell was recorded, and the heat difference at each injection interval was integrated to generate the binding isotherm. Ligands were titrated into ITC buffer as negative controls, and the minimal heat generated from these runs were subtracted from experimental data before further analysis. Calorimetric data were analyzed using the software Origin 7.0 (OriginLab Corporation), where the isotherms were fitted with two-site independent models which provided the best fit for the data among the available models. Affinity, thermodynamics, and stoichiometry were determined from the fitting according to previously described models and fitting procedures (Leavitt & Freire, 2001; Velázquez-Campoy *et al.*, 2004; Velázquez Campoy & Freire, 2005).

The change in heat content from the completion of the i-1 injection to completion of the i injection is plotted against the ligand, which generates the integrated curve (bottom curve). It is calculated by the following equation:

$$\Delta Q(i) = Q(i) + \frac{dV_i}{V_o}\left[\frac{Q\,(i)+Q(i-1)}{2}\right] - Q(i-1)$$

Where Q(i) is the heat of the injection, and Q(i-1) is the heat from previous injection. dV_i is the volume added per injection, into V_o or the changing cell volume.

The total amount of heat is Q, which is a sum of the individual heats per injection. The association constant (K_a) and enthalpy (ΔH) can be determined by the following equation:

$$Q=\frac{n\Delta H P_T V_0}{2}\left[1+\frac{X_t}{nM_t}+\frac{1}{nKM_t}-\sqrt{(1+\frac{X_t}{nM_t}+\frac{1}{nKM_t})^2-\frac{4X_t}{nM_t}}\right]$$

Where P_T is the total protein concentration in the sample cell, corrected for the dilution by the injecting ligand. L_T is the total corrected ligand concentration. n is the stoichiometry. ΔG is determined from K_a using the following equation

$\Delta G = -RT\ln(K_a)$, where $(\frac{1}{K_a})$ is also K_d

$\Delta G = \Delta H - T\Delta S$

So that entropy (ΔS) and Gibb's free energy (ΔG) are also reported.

Binding isotherms are described by the equation $c = K_a[M]N$, where K_a is the association constant, [M] is the total protein concentration in the cell, and N is the stoichiometry of macromolecules. The c values obtained in the thesis are in the range of c values (from ca.1 to 10^3) (Wiseman *et al.*, 1989) that can be used to obtain accurate binding affinity values.

2.5 Dynamic light scattering

Dynamic light scattering (DLS) was used to determine whether the oligomerization state of the protein is altered by the R524Q mutation. This was done in collaboration with Dr. Anson

Chan from Dr. Michael Murphy's lab at UBC. I purified the proteins. Dr. Anson Chan ran DLS and analyzed the DLS data. The protein was diluted to 12.5, 25, 50, 100 or 200μM with ITC buffer into a 50μL mixture, in the absence or presence of ligand (at a 10:1 ratio of ligand to protein). The mixture was spun briefly to get rid of dust debris and precipitation. The samples are run through the DLS three times. Each time, the system is set to perform and average 10 acquisitions. The program Dynamics 7.0 plots the average overall change in intensity over time using the autocorrelation function $g^2(\gamma)=1+\beta e^{-2D_t q^2 \gamma}$ where γ is the time interval that is determined from experimental data by a curve fit, β is the amplitude of the correlation function dependent on the instrument, and q is a scattering vector defined by the optical setup: $q=\frac{4\pi n_0}{\lambda_0}\sin\frac{\theta}{2}$, where n_o is the refractive index, λ_0 is the wavelength of the laser, and θ is the scattering angle.

Finally, D_t is the translational diffusion coefficient that can be solved from the autocorrelation function and inserted into below the Stokes-Einstein equation to solve for particle size.

$$D_h=\frac{K_B T}{3\pi\eta D_t}$$

where k_b is the Boltzmann's constant, T is temperature in Kelvin, and η is dynamic viscosity of water at that temperature. The size of the globular protein is a function of the hydrodynamic diameter (D_h), which depends on the physical size of the protein and its behaviour in solution such as diffusion and viscosity properties. The relationship assumes the protein is a hard sphere traveling in random motion in a non-interacting and viscosity-stable environment. Scattering depends on what happens to pass through the laser at each acquisition and is therefore influenced by sample heterogeneity. DYNAMICS software (Wyatt Technology) is used to determine the distinct populations which are present in the sample and generate a histogram of

signal intensity as a function of hydrodynamic radius. The peak of the histogram is defined by the mean radius, which is calculated by a weighted average of the number of bins comprising the histogram. The width of the peak is the standard deviation of the weighted bin values, also known as the Polydispersity.

2.6 Crystallization and Structure Determination

The C-terminus region of rabbit HCN4 containing the R524Q mutation was crystallized by hanging drop vapor diffusion. The HCN4 R524Q protein was first mixed and incubated with cyclic AMP. The final concentration of protein in mixture was 450μM while the final concentration of cyclic AMP was 5mM. The protein-ligand mixture was mixed with well solution (14% ethanol, 0.2M NaCl, 0.1M sodium citrate pH 4.9) at a ratio of 2:1 and incubated at 4°C.Crystals were obtained after 1-2 weeks at 4°C. Crystals were soaked in a mixture of mother liquor supplemented with 15% MPD and flash frozen. Diffraction data were collected at the Stanford Synchrotron Radiation Lightsource beamline BL 12-2 and processed using HKL3000. The structure was solved by molecular replacement using Phaser (McCoy *et al.*, 2007) with PDB: 3OTF as the search model, using the WT C-terminus as search model (PDB ID 3OTF). Models were completed with iterative cycles of manual model building in COOT (Emsley *et al.*, 2010) and refinement with Refmac5 (Murshudov *et al.*, 2011). Table 2 shows the data and refinement statistics.

Chapter 3: Results

3.1 Cyclic AMP and cGMP bind to the wild type and mutant HCN4 C-terminal tetramer with negative cooperativity and with similar affinities

We wanted to address whether the difference in the EC50 value as shown by published dose-response curves between WT and R524Q mutant is due to a change in binding affinity of cAMP to HCN4 or a change in downstream process of gating. ITC was performed to determine whether the R524Q mutation altered the binding affinity of cyclic AMP to the isolated C-terminus of HCN4 channel. Both parametric test (unpaired t-test) and non-parametric test (Mann-Whitney U test) were performed to determine whether the difference between WT and mutant were statistically significant, and the results aligned for all the binding affinity comparisons and thermodynamics comparisons between the two tests, at a significance level of 0.05. Adding cAMP to purified HCN4 WT or the R524Q mutant produced two clear transitions, which could readily be fit with a two independent binding site model. Binding of cAMP to the WT yielded high and low binding affinity values of 0.04μM and 0.33μM respectively (Table 3.1). The mutant C-terminal protein produced similar binding affinity values of 0.05μM and 0.33μM respectively (Table 3.1). Representative figures of cAMP binding to the C-terminus of WT and R524Q mutants are shown in figure 3.1A.

Because the binding of cGMP to the HCN4 channel may be important in vivo when cAMP concentration is low, we next determined the binding of cGMP to the wild type and mutant HCN4 channel C-terminal tetramer. Binding of cGMP to wild-type HCN4 also produced a biphasic pattern in the binding isotherm which could be best fitted with a two-independent binding site model (Figure 3.1). The high affinity and low affinity binding K_d values for HCN4

WT are 0.20μM and 1.41μM respectively (Table 3.1), which are not significantly different to the K_d values for HCN4 R524Q mutant (0.30μM and 1.29μM respectively).

A thermodynamic analysis of the interaction of WT and R524Q mutant with cAMP and cGMP respectively was also obtained from the ITC measurements (Figure 3.2). For both the mutant and WT, the high affinity binding event was associated with favourable enthalpy and favourable entropy, whereas the low affinity binding event was associated with favourable enthalpy and unfavourable entropy (Figure 3.2). There is no significant difference between enthalpic and entropic contributions to the high affinity or low affinity binding events of cAMP to WT and mutant. For cGMP binding to WT and mutant, no significant difference was observed for the enthalpic and entropic contributions to the low affinity binding events. However, the high affinity delta H value for cGMP binding to mutant was larger in magnitude than that of cGMP binding to WT, and the difference was found to be statistically significant using both unpaired t-test and Mann-Whitney U test. As well, the high affinity entropic contribution for cGMP binding to mutant was smaller in magnitude was found to be significantly lower than that of cGMP binding to WT. This compensated for the difference in enthalpic contributions and resulted in a similar Gibbs free energy of binding, and binding affinity values between the WT and mutant in their binding to cGMP.

		High affinity binding					Low affinity binding				
	n	Kd (μM)	ΔH (kcal/mol)	-TΔS (kcal/mol)	ΔG (kcal/mol)	N	Kd (μM)	ΔH (kcal/mol)	-TΔS (kcal/mol)	ΔG (kcal/mol)	N
Wild type+cAMP	3	0.04±0.008	-5.71±0.54	-4.40±0.44	-10.11±0.11	0.21±0.04	0.33±0.002	12.83±0.19	3.99±0.22	-8.85±0.03	0.93±0.07
Wild type+cGMP	3	0.20±0.02	-0.90±0.40	-8.24±0.41	-9.14±0.06	0.13±0.01	1.41±0.03	13.29±0.41	5.33±0.41	-7.97±0.01	0.91±0.002
R524Q+cAMP	3	0.05±0.01	-3.60±1.14	-6.35±1.26	-9.95±0.14	0.13±0.01	0.33±0.009	12.36±1.03	3.51±1.05	-8.85±0.03	0.96±0.08
R524Q+cGMP	3	0.30±0.10	-2.46±0.18	-6.51±0.21	-8.97±0.20	0.17±0.03	1.29±0.14	13.79±0.31	5.75±0.32	-8.04±0.06	0.87±0.008

Table 3.1. Values for Binding Affinity and Thermodynamic Parameters Describing the Binding of HCN4 WT or R524Q mutant with cyclic AMP and cGMP
Values for mean±SEM are shown as determined from separate experiments (n=number of separate experiments). Thermodynamic parameters (ΔH, -TΔS and ΔG) and stoichiometry values (N) for both high affinity and low affinity binding events are obtained from the best fit of ITC using a two independent-site binding model.

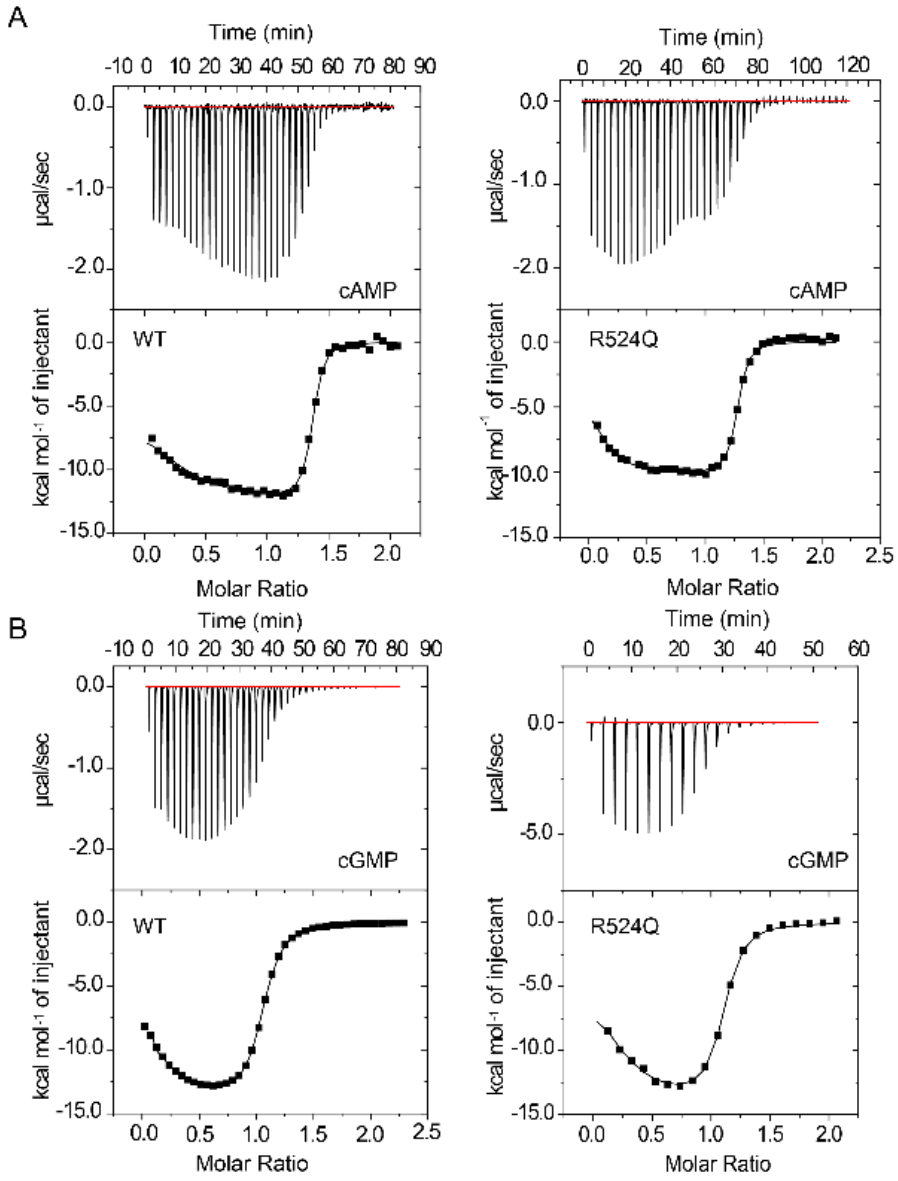

Figure 3.1. The Cyclic Purine Nucleotides cAMP and cGMP bind to the HCN4 C-linker/CNBD with Negative Cooperativity

Plots of heat and binding isotherms produced by injections of 2mM cAMP (A) or 2mM cGMP (B) to 200μM of HCN4 WT C-terminus (left) and R524Q mutant C-terminus (right). The top part of the plot is the raw data arising from injections of cAMP, where each inverted peak shows the heat difference between the sample and reference compartment. As binding sites become saturated, the peaks decrease in their magnitude and eventually plateau to zero. The area under the curve from the top graph is integrated to generate the bottom plot. The solid line through the values represents result of the fit with a two independent binding site model, which yields values for affinity and energetics (ΔG, ΔH and ΔS).

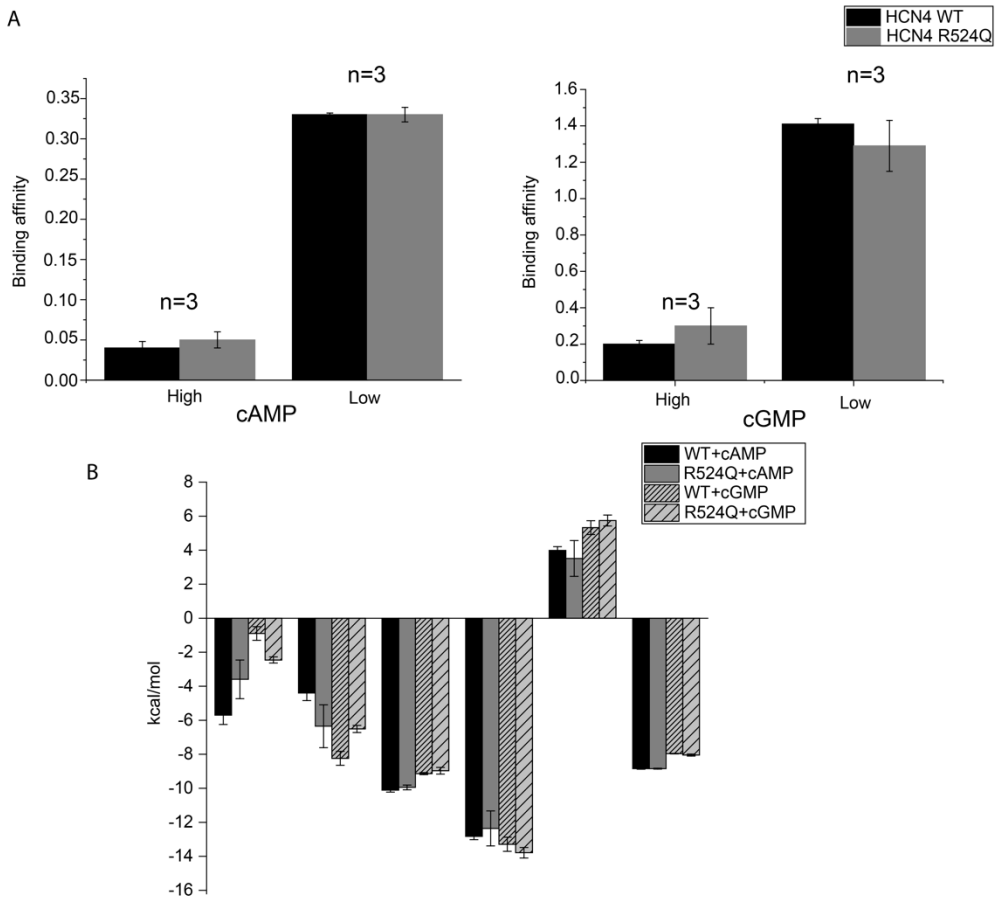

Figure 3.2. Comparisons of binding affinities and thermodynamic values of cAMP binding to WT and R524Q respectively, and cGMP binding to WT and R524Q respectively.

(A) Bar graph showing the high-affinity and low-affinity binding values (K_d) that result from cAMP (left) and cGMP (right) binding to WT and R524Q mutant. The K_d values were derived from fitting of ITC plots using two independent binding site model. Each mean was determined from the average of three ITC binding experiments from two protein purification trials. Values in the graph represent means ± s.e.m. (standard error of means)

(B) Bar groups showing the thermodynamics for the two binding events, a high-affinity and a low-affinity binding event. The same set of data were used as in figure 3.1(B). Values in the graph represent means ± s.e.m.

3.2 Interactions formed by Arg 525 in the full-length Cryo-EM structure

First, we examined the Arginine of interest in the context of full-length Cryo-EM structures. We examined the potential interactions formed by Arg 525 in the full-length structure using the published HCN4 structure in a cAMP-free resting state (7NP3) and in a cAMP-bound resting state (7NP4). In the cAMP-free resting state, no polar interactions exist between the arginine and residues in transmembrane helices (Figure 3.3 A, C). Arg 525 is in proximity with Asp 521 in the same unit, forming a hydrogen bond. In the cAMP-bound resting state, Arg 525 forms a polar interaction with Tyr410 in the TM S4 helix (Figure 3.3 B, D). Different from the cAMP-free state where Asp 521 forms a hydrogen bond with Arg 525, in the cAMP-bound state, Asp 521 forms a hydrogen bond with Arg 418 in the S4-S5 linker. This interaction is significant because in HCN2, the equivalent residues (Arg 339 of the S4-S5 linker and Asp 443 of the C-linker) were found to stabilize the closed state. This raises the possibility that mutating the Arg 525 to glutamine may change the conformation of Asp 521 and therefore its interaction with Arg 418 in the S4-S5 linker.

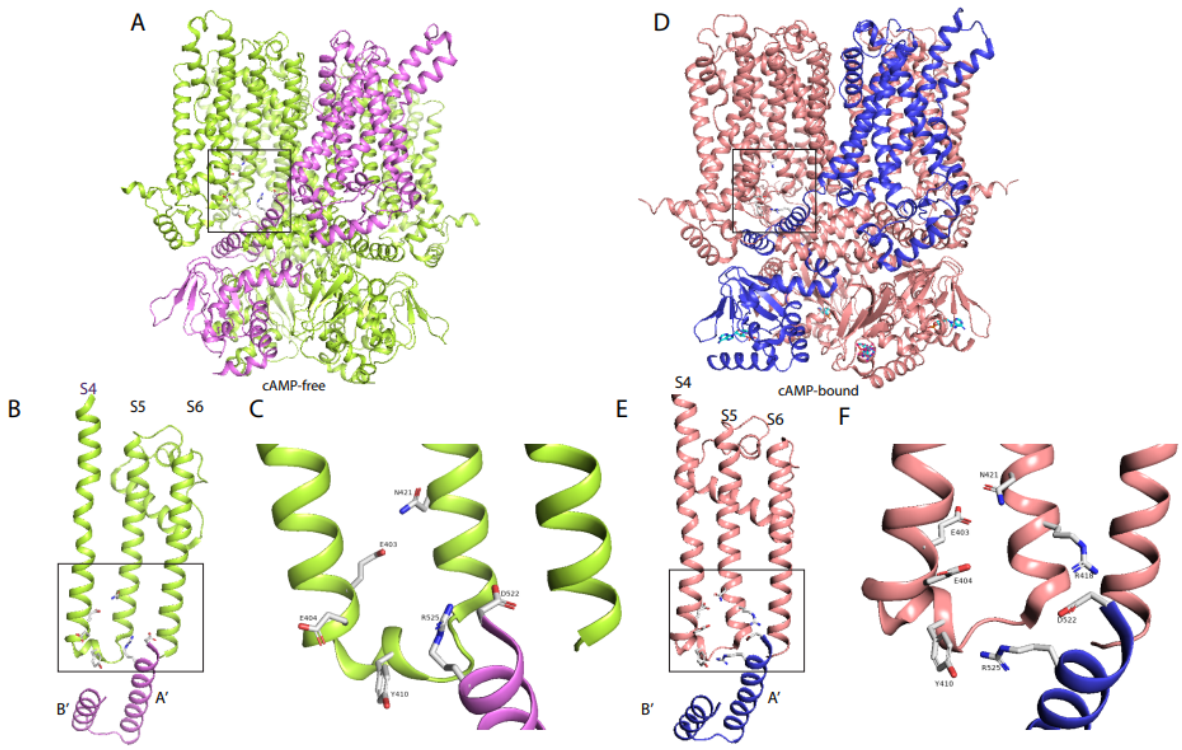

Figure 3.3. Intra-subunit interactions formed by Arg 524 in cAMP-free state (apo) and cAMP bound state of HCN4

(A) Cartoon representations of HCN4 tetramers in a cAMP-free state (PDB code: 7NP3). The first subunit is shown in a different color than the other 3 subunits.
(B) Closer views of elements close to Arginine 525 from (A). Parts of two neighboring subunits are shown. The A' and B' helices of Subunit A are purple and the S4, S5, S6 of the neighboring subunit are in yellow.
(C) A closer view of the close-up from (B). The residues that Arg 525 in Subunit A are in proximity with are shown in sticks and labelled.
(D) Ribbon representations of HCN4 tetramers in a cAMP-bound state (PDB code: 7NP4)
(E) Closer view of elements close to Arginine 525 from (D). The A' and B' helices of Subunit A are shown in blue and the S4, S5, S6 of the neighboring subunit are in pink,
(F) A closer view of the close-up from (E). The residues that Arg 525 in Subunit A are in proximity with are shown in sticks and labelled.

3.3 Crystal structure of the HCN4 R524Q variant

To investigate the impact of R524Q mutant on the crystal structure of the HCN4 C-terminus, we used WT hHCN4 structure as the model (PDB code 3OTF) to conduct molecular replacement and refined the final structure to 2.78Å. The data collection and refinement statistics are shown in table 3.2. Aligning the mutant structure with WT structure (Figure 3.4A) revealed no significant global difference in the structures.

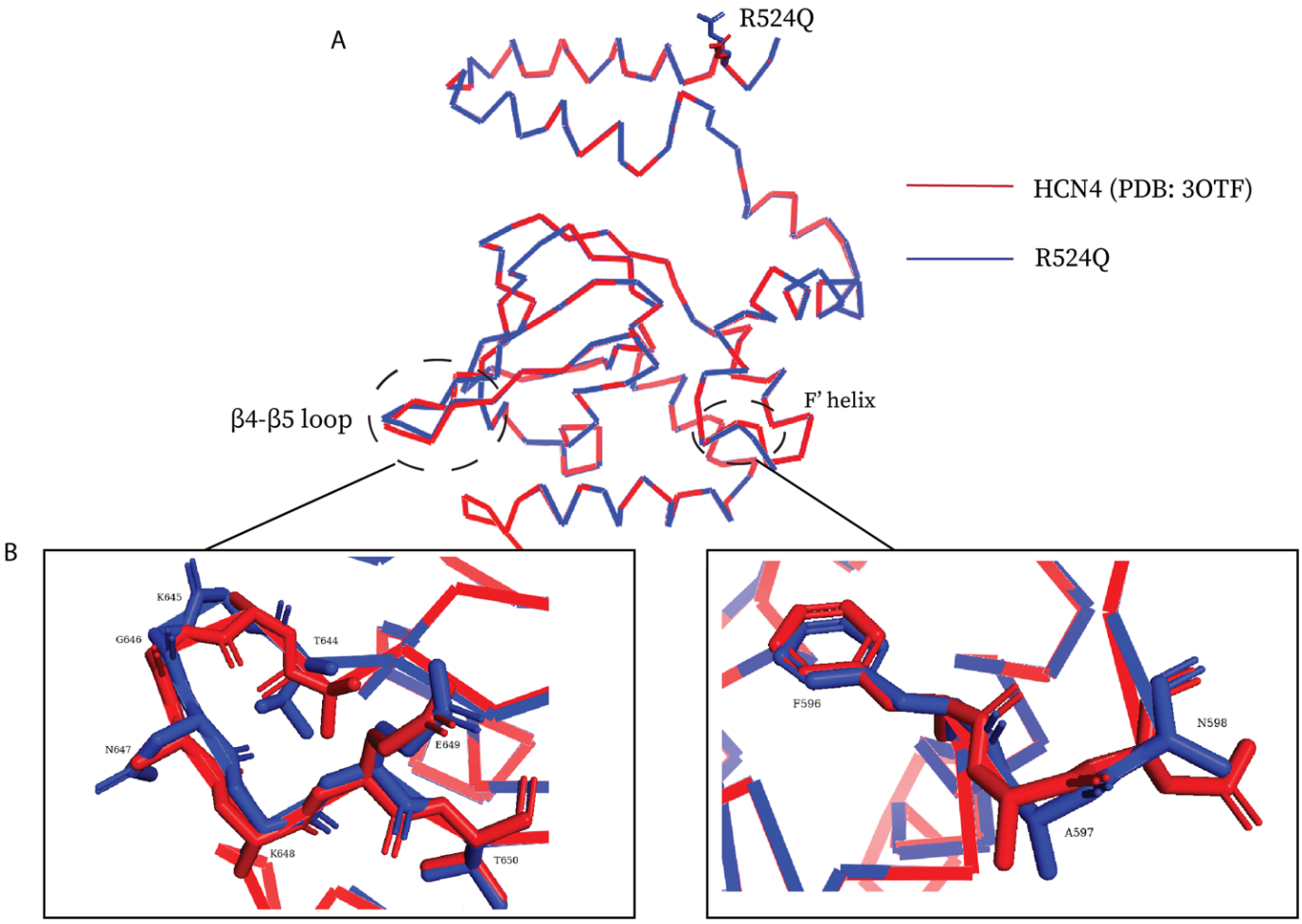

Figure 3.4. Comparison of WT HCN4 C-terminus and R524Q variant structure

(A) Superposition of WT with R524Q, 3OTF is the PDB number of the WT C-terminus crystal structure that has been solved and deposited on PDB. R524Q is the crystal structure that I solved for the mutant C-terminus using X-ray crystallography.

(B) The largest conformation changes due to the R524Q mutation are found in the ß4-ß5 loop and F' helix. The zoomed view of these regions is shown in the dashed boxes, where side chains with the largest conformational changes are shown in sticks.

Aligning WT C-terminus with the mutant C-terminus generated an RMSD of 0.174 over 174 Cα atoms. The position of cAMP is well-aligned between the two structures (Figure 3.4A). However, the loop between β4-β5 from T644 to E649 was disordered (Figure 3.4B). This loop region may play a more prominent role in the coupling between cAMP binding to channel opening rather than cAMP binding itself. As well the F' helix near the end of C-linker (from Phe596 to Ala 599) changed in both its main-chain and side-chain conformation.

3.4 Comparison between crystal and Cryo-EM structures reveal the interaction between C-linker and transmembrane domains that may be impacted by the mutation

To examine the interactions between C-linker and transmembrane elements that are potentially changed by the R524Q mutation, we overlaid the mutant C-terminus structure with the cAMP-bound full-length HCN4 (Figure 3.5 A, C). The salt-bridge between R524 and Tyr410 in the S4 helix is disrupted by the R524Q mutation (Figure 3.5C). It has been previously reported that mutating the equivalent residue of Tyr410 in HCN2 (Tyr 331) prevented channel closure by disrupting an essential interaction with activation gate (Chen *et al.*, 2001b; Decher *et al.*, 2004). Therefore, it is possible that mutating Arg524 to glutamine may shift the closed-open equilibrium to a more open state. The orientation of side chains of Glu524 and Arg524 are also different between the C-terminus crystal structure of the mutant and the full-length WT structure (Figure 3.6 C). To determine whether the difference is a result of the mutation, we also overlaid the crystal structure of the WT C-terminus and the full-length WT (Figure 3.6 A). We found the difference between the side-chain conformations at the start of the C-linker is due to the inherent difference between the crystal structure of isolated domains and full-length cryo-EM structure (Figure 3.6 A, B, C). This can possibly be attributed to the lack of constraints from the transmembrane domains in crystal structures of isolated domains (Lee & MacKinnon, 2017).

Table 3.2 Data Collection and Refinement Statistics for HCN4 R524Q mutant C-linker/CNBD crystallized with cyclic AMP

Space group	I 4 2 2
Cell dimensions	
a,b,c (Å)	69.14 69.14 193.256
α,ß,γ (°)	90 90 90
Resolution (Å)	34.57-2.78 (2.88-2.78)
R_{pim}	0.05576 (0.9584)
I/σI	15.59 (1.61)
Completeness (%)	99.49 (96.22)
Redundancy	12.0 (11.5)
Reflections used in refinement	6256 (586)
R_{work}/R_{free}	0.2604/0.3185
No. of atoms	
Protein	1459
Ligand	22
B factors	
Protein	90.03
Ligand	97.46
Ramachandran favored (%)	94.18
Ramachandran allowed (%)	5.82
Ramachandran outliers (%)	0.00
Root-mean-square deviations	
Bond lengths (Å)	0.014
Bond angles (°)	1.86

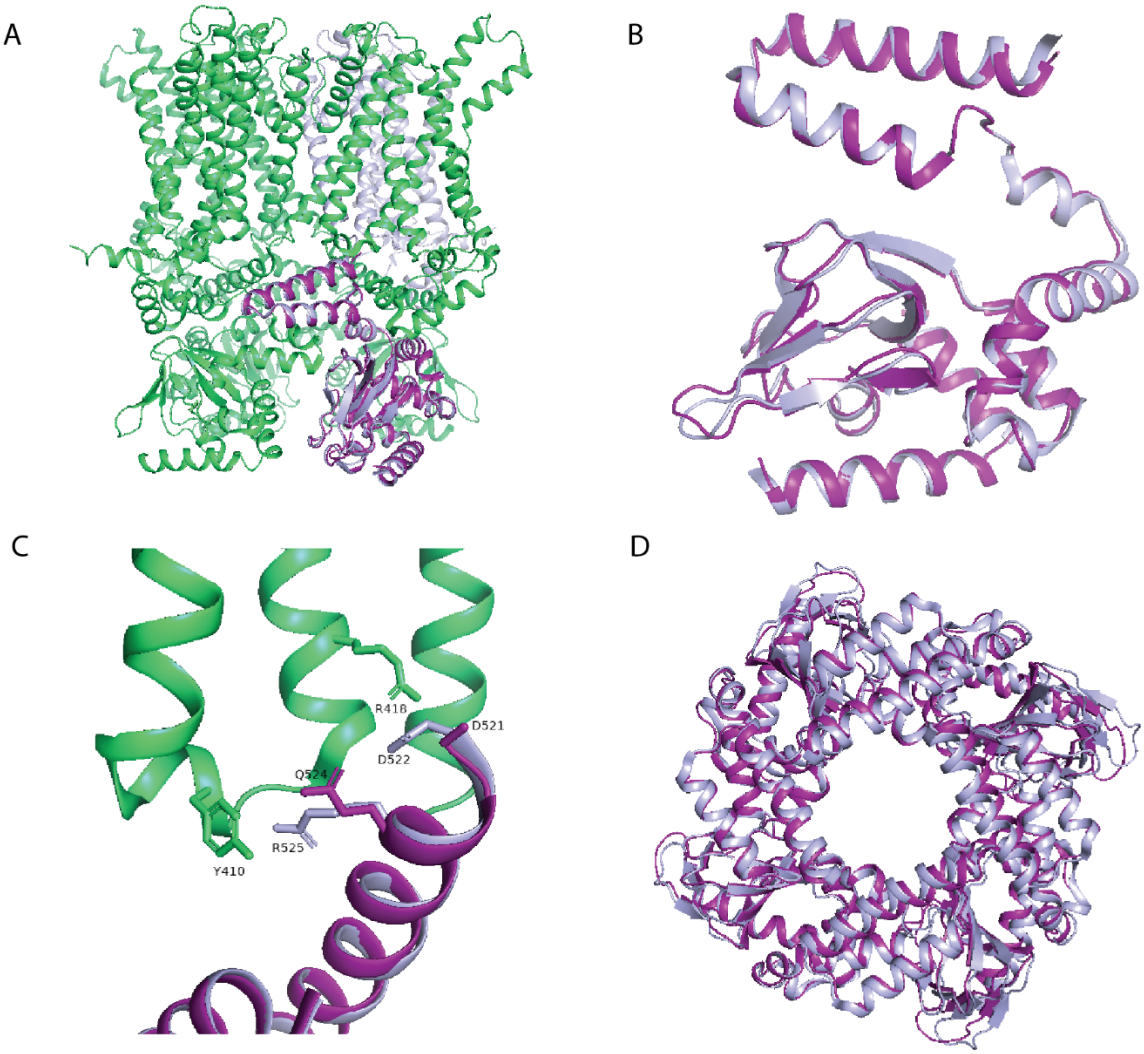

Figure 3.5. Superposition of cAMP-bound full-length HCN4 (PDB: 7NP4) and crystal structure of HCN4 C-terminus of the R524Q mutant

(A) Cartoon representation of full-length cAMP-bound WT HCN4 aligned with crystal structure of HCN4 C-terminus. The first subunit of cryo-EM structure is shown in blue and crystal structure of the R524Q mutant is in purple. The other three subunits of full-length HCN4 are shown in green.

(B) C-terminus close-up of figure (A). The C-terminus of first subunit of full-length HCN4 (blue) aligned with crystal structure of HCN4 C-terminus (purple).

(C) Close-up of figure (A) showing the inter-subunit interactions close to Arginine or Glutamine for WT cryo-EM structure and R524Q mutant C-terminus structure respectively. The A' and B' helices of Subunit A in full-length HCN4 are shown in blue and the S4, S5, S6 of the neighboring subunit are in purple. The A' and B' helices of R524Q mutant C-terminus crystal structure are shown in purple and aligned with A' and

B’ helices of WT cryo-EM structure. R525 in the full-length channel is equivalent to Q524 in the mutant crystal structure, and D522 in the full-length channel is equivalent to D521 in the crystal structure.

(D) Superposition of the cytoplasmic tetramers from the cAMP-bound cryo-EM structure (blue) and from the mutant crystal structure of isolated domain (purple). (D) is viewed from the extracellular side.

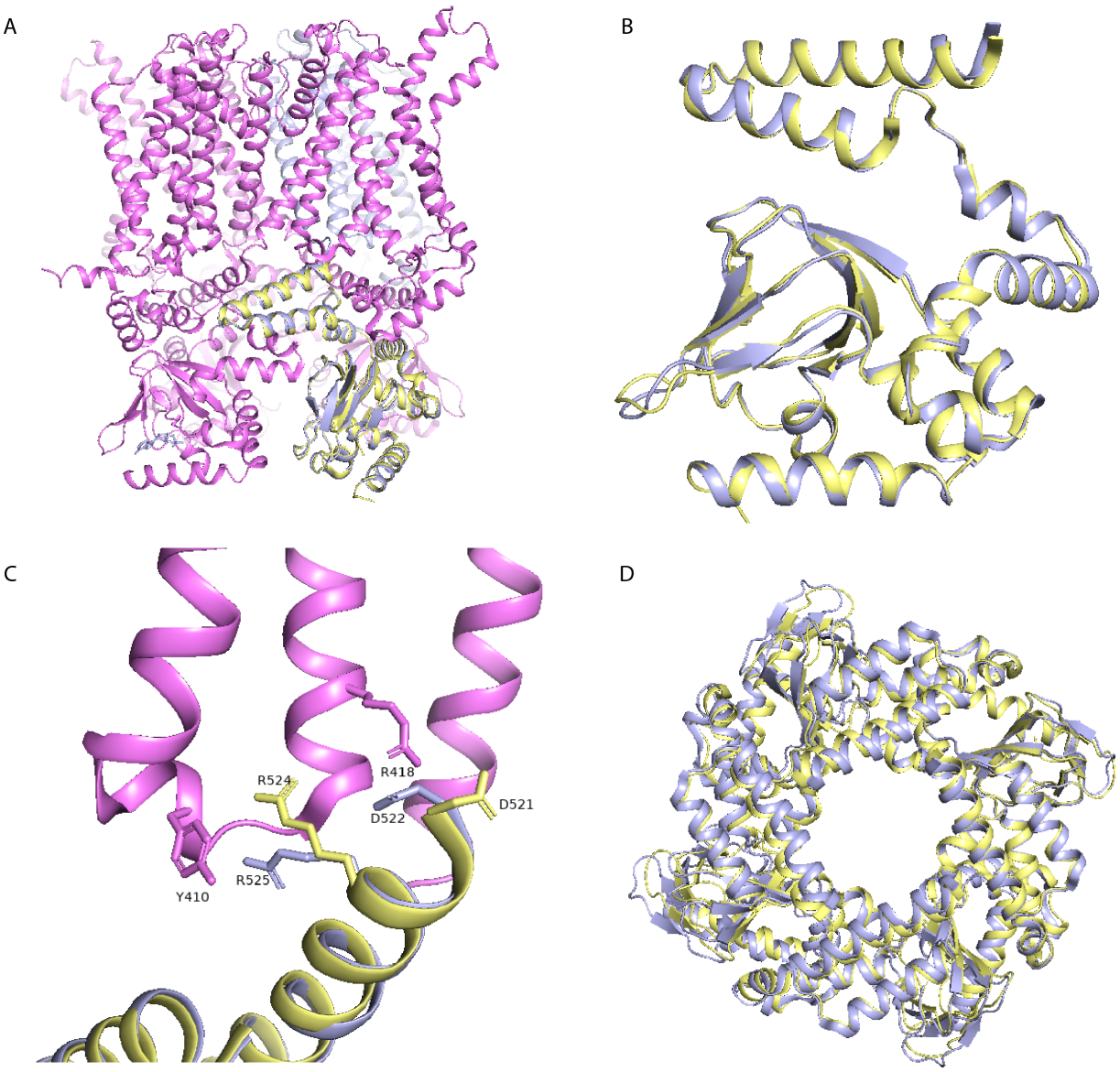

Figure 3.6. Superposition of cAMP-bound full-length HCN4 (PDB: 7NP4) and crystal structure of WT HCN4 C-terminus (PDB: 3OTF)

(A) Cartoon representation of full-length cAMP-bound HCN4 aligned with crystal structure of HCN4 C-terminus. The first subunit of full-length HCN4 is shown in blue and overlaid crystal structure in yellow. The other three subunits of full-length HCN4 are shown in purple.

(B) C-terminus close-up of figure (A). The C-terminus of first subunit of full-length HCN4 (blue) aligned with crystal structure of HCN4 C-terminus (yellow).

(C) Close-up of figure (A) showing the inter-subunit interactions close to Arginine for full-length HCN4 and C-terminus structure respectively. The A' and B' helices of Subunit A

in full-length HCN4 are shown in blue and the S4, S5, S6 of the neighboring subunit are in purple. The A' and B' helices of HCN4 C-terminus crystal structure are shown in yellow and aligned with those of the full-length HCN4 channel. R525 in the full-length channel is equivalent to R524 in the crystal structure, and D522 in the full-length channel is equivalent to D521 in the crystal structure.

(D) Superposition of the cytoplasmic tetramers from the cAMP-bound cryo-EM structure (blue) and from crystal structure of isolated domain (yellow). A tetrameric assembly was built based on crystallographic symmetry in pymol. (D) is viewed from the extracellular side.

3.5 R524Q mutation does not significantly impact the self-association of the HCN4 C-linker/CNBD that is promoted by cyclic AMP and cyclic GMP, as measured by dynamic light scattering

We also performed dynamic light scattering to examine whether the oligomerization state of HCN4 C-terminus is impacted by the mutation. Previous studies on the HCN2 C-terminus has shown that the apparent molecular weight of the HCN2 C-terminus is increased with higher concentration of protein even in the absence of ligand, showing that high protein concentrations promote the formation of tetramers (Chow *et al.*, 2012a; Ng *et al.*, 2016). In addition, cyclic AMP was found to promote the oligomerization of HCN2 C-terminus except for the highest concentration, with its effect being the most pronounced at lower concentrations (Chow *et al.*, 2012a; Ng *et al.*, 2016). My results showed that, similar to HCN2 C-terminus, the apparent molecular weight of the HCN4 C-terminus also increases with higher protein concentration and cyclic AMP promotes the oligomerization especially at lower protein concentration (Figure 3.7). The mutation does not change the oligomerization state of protein, both in the presence and absence of cyclic AMP (Figure 3.7). Cyclic GMP also promotes the oligomerization of HCN4 C-terminus to a similar extent as cyclic AMP, with a larger effect at the highest protein concentration tested (200μM). The R524Q mutation increases the

oligomerization of HCN4 C-terminus in the presence of cyclic GMP at a protein concentration of 50μM and 100μM compared to WT; however, a significant difference was not observed at other protein concentrations. More trials need to be conducted in order to determine whether the difference is significant.

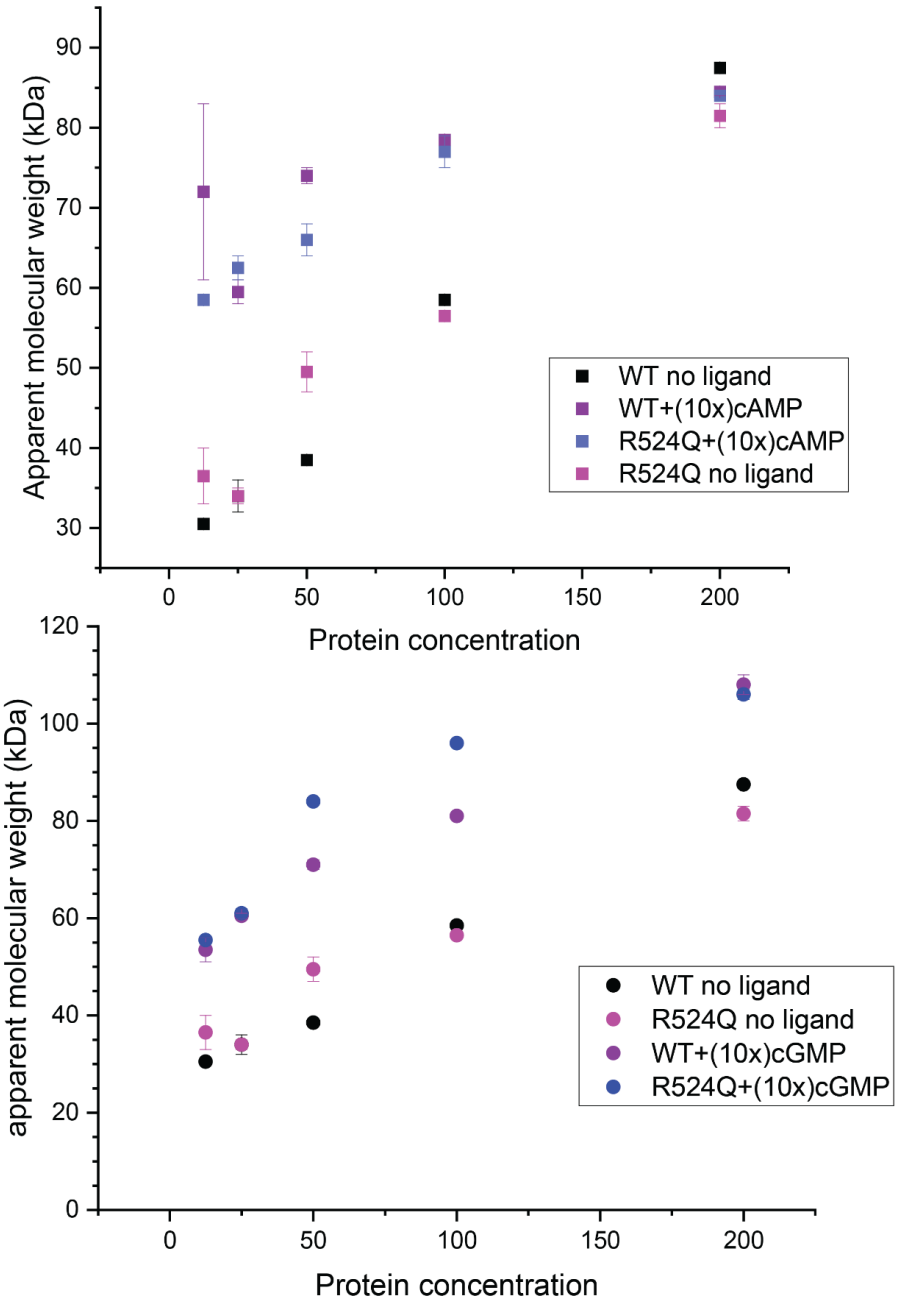

Figure 3.7. Oligomerization of the HCN4 C-linker/CNBD is promoted by cAMP and cGMP and not significantly changed by R524Q mutation

Plots of estimated average molecular weight versus concentration of purified HCN4 C-linker/CNBD protein are shown. Values represent means ± SEM, determined from three DLS runs using one preparation of purified protein.

Chapter 4: Discussion

4.1 The shift in R524Q dose-response curve is not a result of change in direct binding affinity

Our study of the R524Q mutation demonstrated that the increase in potency (as indicated by a lower EC50) from functional studies is not due to changes in direct cAMP binding affinity, but rather downstream processes that couple cAMP binding to channel gating. In addition, our study raises the possibility that mutations far away from the cAMP-binding site could also change the stability of the loop on the cAMP entry path.

The R524Q mutation in the HCN4 is the first discovered gain-of-function mutation in HCN4 and is associated with Inappropriate Sinus Tachycardia (Baruscotti *et al.*, 2017). The mutation does not change how the channel gates in the absence of cAMP or the maximal effect of cAMP but shifts the concentration response curve to lower concentrations of cyclic AMP.

To determine whether the increase in potency in the mutant is due to the increase in direct binding affinity or other factors, we carried out binding measurements on the tetrameric C-terminus (C-linker and CNBD) of WT and R524Q HCN4. Both wild-type and mutant bind to cAMP and cGMP with negative cooperativity at a high protein concentration. The high affinity and low binding affinity values of both cAMP and cGMP are not significantly changed by the mutation. This is not surprising given that the mutation is located at the start of C-linker, far away from the cAMP binding pocket. Therefore, we hypothesize that the mutation changes the way information from cAMP binding is transmitted to facilitate channel opening. This is also indirectly substantiated by the hill coefficients of the concentration-response curve (0.55, 0.41 and 0.36 for WT, WT-R524Q and R524Q respectively), indicating a difference in the gating parameters between WT and mutant channels (Baruscotti *et al.*, 2017).

4.2 The mutation disrupts a salt bridge between TM domain and C-linker that may impact gating

To investigate whether the R524Q would perturb biochemical interactions in the full-length HCN4 structure, we examined the cryo-EM structures for HCN4 in cAMP-free and cAMP-bound states that were recently published (Saponaro *et al.*, 2021). These structures give us insight into the unique contact between the C-linker and TM domain which distinguishes HCN4 from HCN1 cryo-EM structure. The S4-S5 linker develops a full-helical turn which builds a tetrad arrangement between two residues in the S4-S5 linker and two residues in the C-linker domain. Binding of cAMP to CNBD results in a rotation of A' helix and B' helix which enables the formation of a salt bridge between the arginine of interest (Arginine 525) and Tyrosine 410 in the S4-S5 linker, which is absent in the cAMP-free structure. This salt bridge is significant because the interface between transmembrane domains and cytosolic domains were found to regulate HCN channel gating (Chen *et al.*, 2001a; Kwan *et al.*, 2012; Weißgraeber *et al.*, 2017; Porro *et al.*, 2019). Y331, the equivalent residue of Y410 in HCN2, was found to be essential in coupling voltage sensor movement and channel opening and closing (Chen *et al.*, 2001a). The C-linker, where Arg525 is located, couples channel gating to the ligand-binding domain. The cryo-EM structures further highlighted a pathway that is probably unique to HCN4, whereby the interaction between the S4-S5 and the C-linker is critical to transmit the cAMP-binding information between the C-linker and the VSD (Saponaro *et al.*, 2021). Therefore, by disrupting a salt bridge between C-linker and the S4-S5 linker, the R524Q mutation may disrupt the facilitative role of S4-S5 linker in coupling the cAMP effect between the C-linker and the voltage-sensing domain, impacting the coupling between ligand binding and channel opening.

4.3 A possible role of lipids

It is interesting to note the presence of lipids in the cryo-EM structures. Non-protein densities are present in proximity to the lower part of the S4 helix, where it connects to the S4-S5 linker. Two putative lipids encircle helix S5. The distribution of lipids is similar between the holo HCN4 cryo-EM structures (7NP4) that are solved by Saponaro et al. (Saponaro *et al.*, 2021) and in the HCN4 holo structure solved by the Structural Genomics Consortium (PDB: 6GYO). Interestingly, the presence and absence of lipids associated with S4 and S5 were found to associate with a closed and open pore respectively. It is therefore likely that lipids stabilize the HCN4 structure in a closed pore state (Saponaro *et al.*, 2021). In heterologous expressed channels, lipid rafts were found to shift the current activation curve to more negative voltages (Barbuti *et al.*, 2004). Since the Arginine of interest is near lipids including phosphatidylethanolamine and phosphatidylcholine (Barbuti *et al.*, 2004), it remains to be investigated whether the mutation would alter the lipid distribution and whether the alteration would be significant for gating.

4.4 Differences in crystal structures between WT C-terminus and R524Q C-terminus

We performed X-ray crystallography to investigate potential structural changes in the C-terminus because of the mutation. Crystallographic study of the R524Q mutant showed no significant global difference between the WT C-terminus and mutant C-terminus. However, local structure variation was observed in the loop between ß4 and ß5, and in the F' helix. The ß4- ß5 loop constitutes the cAMP entry-exit pathway and forms extensive contact with the purine ring of cAMP (Zagotta et al., 2003; Xu et al., 2010). Significantly, ß4- ß5 loop also constitutes a major structural deviation between the C-terminus of HCN1, HCN2 and HCN4 (Lolicato et al, 2011). A previous study with another mutation in HCN4 C-terminus showed that mutating a

residue, S672R in the cAMP binding pocket changes the conformation of ß4- ß5 loop (Xu et al., 2012). Since the location of R524Q mutation is at the start of the C-linker and far away from the loop and cAMP binding pocket, it remains to be investigated how the impact of mutation gets transmitted to the ß4- ß5 loop and F' helix.

4.5 Limitations and future directions

A major limitation of this study is that the results of our studies and similar studies may be influenced by the expression system and protein purification methods. A bacterial expression system using *E.coli* is used for our study. The post-translational modification of proteins would differ from those expressed in a mammalian expressions system (e.g. HEK cells used in the cryo-EM study of HCN4). In addition, due to our purification methods, lipids were absent which could also potentially result in a different conformation of the protein compared to a system with lipids (e.g. (Saponaro *et al.*, 2021). This limitation could be mitigated by repeating the experiment in HEK cells, expressing the full-length protein, and measuring the binding affinity of cAMP to the full-length protein.

Also, since binding measurements were conducted on the isolated HCN C-terminus instead of on the full-length channel, it remains to be investigated whether the binding values of WT and R524Q mutant channels will also be similar in the full-length channel. However, as discussed previously and shown in figure 1.7 the measured equilibrium association constants derived from full-length HCN SM measurements in ZMW are similar to those obtained from ITC measurements using the C-terminus piece. Therefore, I predict the trend potentially observed in the full-length channel will also be similar.

In addition, given the mutation is at the start of C-terminus, conformation of amino acid residues at the start of C-linker may be different in the crystal structure compared to full-length

structure, due to the lack of constraints from transmembrane domains. To address this limitation, the cryo-EM structure of full-length HCN4 carrying the R524Q mutation could be solved and compared to the WT full-length structure.

A close examination of the cryo-EM structure of full-length HCN4 shows that the R525-Tyr410 salt bridge is potentially affected by the mutation. To better understand the impact of the affected salt bridge, future studies could potentially mutate both residues in full-length channels and measure the gating parameters. The binding affinities between WT and R524Q are similar, therefore the differences in concentration-response relations are likely due to differences in the rates of channel opening and closing. Because it was previously reported that mutating the equivalent residue of Tyr410 in HCN2 prevented channel closure at more positive voltages (Chen et al., 2001b; Decher et al., 2004). I predict that the disruption of R525-Tyr410 interaction in full-length channel will increase the channel opening probability at more positive voltages. This might explain the shift of dose-response curve to lower concentrations of cAMP with the mutation, in the absence of changes in binding affinity.

Crystallographic investigations indicate that the R524Q mutation causes limited changes in the structure of HCN4 C-terminus, but its effects on protein dynamics are not well understood. Further studies using MD simulations or NMR experiments to characterize the dynamic motion of mutant protein in its binding to cAMP will be helpful.

Bibliography

Accili EA, Robinson RB & DiFrancesco D. (1997). Properties and modulation of If in newborn versus adult cardiac SA node. *Am J Physiol* **272,** H1549-1552.

Altomare C, Bucchi A, Camatini E, Baruscotti M, Viscomi C, Moroni A & DiFrancesco D. (2001). Integrated allosteric model of voltage gating of HCN channels. *J Gen Physiol* **117,** 519-532.

Barbuti A, Baruscotti M & DiFrancesco D. (2007). The pacemaker current: from basics to the clinics. *J Cardiovasc Electrophysiol* **18,** 342-347.

Barbuti A, Gravante B, Riolfo M, Milanesi R, Terragni B & DiFrancesco D. (2004). Localization of pacemaker channels in lipid rafts regulates channel kinetics. *Circ Res* **94,** 1325-1331.

Baruscotti M, Barbuti A & Bucchi A. (2010). The cardiac pacemaker current. *J Mol Cell Cardiol* **48,** 55-64.

Baruscotti M, Bucchi A & Difrancesco D. (2005). Physiology and pharmacology of the cardiac pacemaker ("funny") current. *Pharmacol Ther* **107,** 59-79.

Baruscotti M, Bucchi A, Milanesi R, Paina M, Barbuti A, Gnecchi-Ruscone T, Bianco E, Vitali-Serdoz L, Cappato R & DiFrancesco D. (2017). A gain-of-function mutation in the cardiac pacemaker HCN4 channel increasing cAMP sensitivity is associated with familial Inappropriate Sinus Tachycardia. *Eur Heart J* **38,** 280-288.

Bigger JT & Reiffel JA. (1979). Sick sinus syndrome. *Annu Rev Med* **30,** 91-118.

Boyett MR, Honjo H & Kodama I. (2000). The sinoatrial node, a heterogeneous pacemaker structure. *Cardiovasc Res* **47,** 658-687.

Brewster AL, Chen Y, Bender RA, Yeh A, Shigemoto R & Baram TZ. (2007). Quantitative analysis and subcellular distribution of mRNA and protein expression of the hyperpolarization-activated cyclic nucleotide-gated channels throughout development in rat hippocampus. *Cereb Cortex* **17,** 702-712.

Brown HF, DiFrancesco D & Noble SJ. (1979). How does adrenaline accelerate the heart? *Nature* **280,** 235-236.

Chen J, Mitcheson JS, Tristani-Firouzi M, Lin M & Sanguinetti MC. (2001a). The S4-S5 linker couples voltage sensing and activation of pacemaker channels. *Proc Natl Acad Sci U S A* **98,** 11277-11282.

Chen S, Wang J & Siegelbaum SA. (2001b). Properties of hyperpolarization-activated pacemaker current defined by coassembly of HCN1 and HCN2 subunits and basal modulation by cyclic nucleotide. *J Gen Physiol* **117,** 491-504.

Chow SS, Van Petegem F & Accili EA. (2012a). Energetics of cyclic AMP binding to HCN channel C terminus reveal negative cooperativity. *J Biol Chem* **287,** 600-606.

Chow SS, Van Petegem F & Accili EA. (2012b). Energetics of cyclic AMP binding to HCN channel C terminus reveal negative cooperativity. *J Biol Chem* **287,** 600-606.

Decher N, Chen J & Sanguinetti MC. (2004). Voltage-dependent gating of hyperpolarization-activated, cyclic nucleotide-gated pacemaker channels: molecular coupling between the S4-S5 and C-linkers. *J Biol Chem* **279,** 13859-13865.

DiFrancesco D. (1981). A new interpretation of the pace-maker current in calf Purkinje fibres. *J Physiol* **314,** 359-376.

DiFrancesco D. (1986). Characterization of single pacemaker channels in cardiac sino-atrial node cells. *Nature* **324,** 470-473.

DiFrancesco D. (1993). Pacemaker mechanisms in cardiac tissue. *Annu Rev Physiol* **55,** 455-472.

DiFrancesco D. (2010). The role of the funny current in pacemaker activity. *Circ Res* **106,** 434-446.

DiFrancesco D, Ferroni A, Mazzanti M & Tromba C. (1986). Properties of the hyperpolarizing-activated current (if) in cells isolated from the rabbit sino-atrial node. *J Physiol* **377,** 61-88.

DiFrancesco D & Mangoni M. (1994). Modulation of single hyperpolarization-activated channels (i(f)) by cAMP in the rabbit sino-atrial node. *J Physiol* **474,** 473-482.

DiFrancesco D & Ojeda C. (1980). Properties of the current if in the sino-atrial node of the rabbit compared with those of the current iK, in Purkinje fibres. *J Physiol* **308,** 353-367.

DiFrancesco D & Tortora P. (1991). Direct activation of cardiac pacemaker channels by intracellular cyclic AMP. *Nature* **351,** 145-147.

DiFrancesco D & Tromba C. (1988). Muscarinic control of the hyperpolarization-activated current (if) in rabbit sino-atrial node myocytes. *J Physiol* **405,** 493-510.

Duhme N, Schweizer PA, Thomas D, Becker R, Schröter J, Barends TR, Schlichting I, Draguhn A, Bruehl C, Katus HA & Koenen M. (2013). Altered HCN4 channel C-linker interaction is associated with familial tachycardia-bradycardia syndrome and atrial fibrillation. *Eur Heart J* **34,** 2768-2775.

Easterling M, Rossi S, Mazzella AJ & Bressan M. (2021). Assembly of the Cardiac Pacemaking Complex: Electrogenic Principles of Sinoatrial Node Morphogenesis. *J Cardiovasc Dev Dis* **8**.

Elinder F, Männikkö R, Pandey S & Larsson HP. (2006). Mode shifts in the voltage gating of the mouse and human HCN2 and HCN4 channels. *J Physiol* **575,** 417-431.

Emsley P, Lohkamp B, Scott WG & Cowtan K. (2010). Features and development of Coot. *Acta Crystallogr D Biol Crystallogr* **66,** 486-501.

Fenske S, Krause SC, Hassan SI, Becirovic E, Auer F, Bernard R, Kupatt C, Lange P, Ziegler T, Wotjak CT, Zhang H, Hammelmann V, Paparizos C, Biel M & Wahl-Schott CA. (2013). Sick sinus syndrome in HCN1-deficient mice. *Circulation* **128,** 2585-2594.

Flynn GE, Black KD, Islas LD, Sankaran B & Zagotta WN. (2007). Structure and rearrangements in the carboxy-terminal region of SpIH channels. *Structure* **15,** 671-682.

Gauss R, Seifert R & Kaupp UB. (1998). Molecular identification of a hyperpolarization-activated channel in sea urchin sperm. *Nature* **393,** 583-587.

Hauswirth O, Noble D & Tsien RW. (1968). Adrenaline: mechanism of action on the pacemaker potential in cardiac Purkinje fibers. *Science* **162,** 916-917.

Herrmann S, Layh B & Ludwig A. (2011). Novel insights into the distribution of cardiac HCN channels: an expression study in the mouse heart. *J Mol Cell Cardiol* **51,** 997-1006.

Ishii TM, Takano M, Xie LH, Noma A & Ohmori H. (1999). Molecular characterization of the hyperpolarization-activated cation channel in rabbit heart sinoatrial node. *J Biol Chem* **274,** 12835-12839.

Kassebaum DG & Van Dyke AR. (1966). Electrophysiological effects of isoproterenol on Purkinje fibers of the heart. *Circ Res* **19,** 940-946.

Kusch J, Thon S, Schulz E, Biskup C, Nache V, Zimmer T, Seifert R, Schwede F & Benndorf K. (2011). How subunits cooperate in cAMP-induced activation of homotetrameric HCN2 channels. *Nat Chem Biol* **8,** 162-169.

Kwan DC, Prole DL & Yellen G. (2012). Structural changes during HCN channel gating defined by high affinity metal bridges. *J Gen Physiol* **140,** 279-291.

Laish-Farkash A, Glikson M, Brass D, Marek-Yagel D, Pras E, Dascal N, Antzelevitch C, Nof E, Reznik H, Eldar M & Luria D. (2010). A novel mutation in the HCN4 gene causes symptomatic sinus bradycardia in Moroccan Jews. *J Cardiovasc Electrophysiol* **21,** 1365-1372.

Leavitt S & Freire E. (2001). Direct measurement of protein binding energetics by isothermal titration calorimetry. *Curr Opin Struct Biol* **11,** 560-566.

Lee CH & MacKinnon R. (2017). Structures of the Human HCN1 Hyperpolarization-Activated Channel. *Cell* **168,** 111-120.e111.

Lolicato M, Nardini M, Gazzarrini S, Möller S, Bertinetti D, Herberg FW, Bolognesi M, Martin H, Fasolini M, Bertrand JA, Arrigoni C, Thiel G & Moroni A. (2011). Tetramerization dynamics of C-terminal domain underlies isoform-specific cAMP gating in hyperpolarization-activated cyclic nucleotide-gated channels. *J Biol Chem* **286,** 44811-44820.

Ludwig A, Budde T, Stieber J, Moosmang S, Wahl C, Holthoff K, Langebartels A, Wotjak C, Munsch T, Zong X, Feil S, Feil R, Lancel M, Chien KR, Konnerth A, Pape HC, Biel M & Hofmann F. (2003). Absence epilepsy and sinus dysrhythmia in mice lacking the pacemaker channel HCN2. *EMBO J* **22,** 216-224.

Ludwig A, Zong X, Jeglitsch M, Hofmann F & Biel M. (1998). A family of hyperpolarization-activated mammalian cation channels. *Nature* **393,** 587-591.

Ludwig A, Zong X, Stieber J, Hullin R, Hofmann F & Biel M. (1999). Two pacemaker channels from human heart with profoundly different activation kinetics. *EMBO J* **18,** 2323-2329.

Macri V, Mahida SN, Zhang ML, Sinner MF, Dolmatova EV, Tucker NR, McLellan M, Shea MA, Milan DJ, Lunetta KL, Benjamin EJ & Ellinor PT. (2014). A novel trafficking-defective HCN4 mutation is associated with early-onset atrial fibrillation. *Heart Rhythm* **11,** 1055-1062.

McCoy AJ, Grosse-Kunstleve RW, Adams PD, Winn MD, Storoni LC & Read RJ. (2007). Phaser crystallographic software. *J Appl Crystallogr* **40,** 658-674.

Milanesi R, Baruscotti M, Gnecchi-Ruscone T & DiFrancesco D. (2006). Familial sinus bradycardia associated with a mutation in the cardiac pacemaker channel. *N Engl J Med* **354,** 151-157.

Milano A, Vermeer AM, Lodder EM, Barc J, Verkerk AO, Postma AV, van der Bilt IA, Baars MJ, van Haelst PL, Caliskan K, Hoedemaekers YM, Le Scouarnec S, Redon R, Pinto YM, Christiaans I, Wilde AA & Bezzina CR. (2014). HCN4 mutations in multiple families with bradycardia and left ventricular noncompaction cardiomyopathy. *J Am Coll Cardiol* **64,** 745-756.

Moosmang S, Stieber J, Zong X, Biel M, Hofmann F & Ludwig A. (2001). Cellular expression and functional characterization of four hyperpolarization-activated pacemaker channels in cardiac and neuronal tissues. *Eur J Biochem* **268,** 1646-1652.

Moroni A, Gorza L, Beltrame M, Gravante B, Vaccari T, Bianchi ME, Altomare C, Longhi R, Heurteaux C, Vitadello M, Malgaroli A & DiFrancesco D. (2001). Hyperpolarization-activated cyclic nucleotide-gated channel 1 is a molecular determinant of the cardiac pacemaker current I(f). *J Biol Chem* **276,** 29233-29241.

Murshudov GN, Skubák P, Lebedev AA, Pannu NS, Steiner RA, Nicholls RA, Winn MD, Long F & Vagin AA. (2011). REFMAC5 for the refinement of macromolecular crystal structures. *Acta Crystallogr D Biol Crystallogr* **67,** 355-367.

Neyton J & Miller C. (1988). Potassium blocks barium permeation through a calcium-activated potassium channel. *J Gen Physiol* **92,** 549-567.

Ng LCT, Putrenko I, Baronas V, Van Petegem F & Accili EA. (2016). Cyclic Purine and Pyrimidine Nucleotides Bind to the HCN2 Ion Channel and Variably Promote C-Terminal Domain Interactions and Opening. *Structure* **24,** 1629-1642.

Ng LCT, Zhuang M, Van Petegem F, Li YX & Accili EA. (2019). Binding and structural asymmetry governs ligand sensitivity in a cyclic nucleotide-gated ion channel. *J Gen Physiol* **151,** 1190-1212.

Nof E, Luria D, Brass D, Marek D, Lahat H, Reznik-Wolf H, Pras E, Dascal N, Eldar M & Glikson M. (2007). Point mutation in the HCN4 cardiac ion channel pore affecting synthesis, trafficking, and functional expression is associated with familial asymptomatic sinus bradycardia. *Circulation* **116,** 463-470.

Olshansky B & Sullivan RM. (2019). Inappropriate sinus tachycardia. *Europace* **21,** 194-207.

Osterrieder W, Brum G, Hescheler J, Trautwein W, Flockerzi V & Hofmann F. (1982). Injection of subunits of cyclic AMP-dependent protein kinase into cardiac myocytes modulates Ca2+ current. *Nature* **298,** 576-578.

Popovych N, Sun S, Ebright RH & Kalodimos CG. (2006). Dynamically driven protein allostery. *Nat Struct Mol Biol* **13,** 831-838.

Porro A, Saponaro A, Gasparri F, Bauer D, Gross C, Pisoni M, Abbandonato G, Hamacher K, Santoro B, Thiel G & Moroni A. (2019). The HCN domain couples voltage gating and cAMP response in hyperpolarization-activated cyclic nucleotide-gated channels. *Elife* **8**.

Robinson RB & Siegelbaum SA. (2003). Hyperpolarization-activated cation currents: from molecules to physiological function. *Annu Rev Physiol* **65,** 453-480.

Santoro B, Liu DT, Yao H, Bartsch D, Kandel ER, Siegelbaum SA & Tibbs GR. (1998). Identification of a gene encoding a hyperpolarization-activated pacemaker channel of brain. *Cell* **93,** 717-729.

Saponaro A, Bauer D, Giese MH, Swuec P, Porro A, Gasparri F, Sharifzadeh AS, Chaves-Sanjuan A, Alberio L, Parisi G, Cerutti G, Clarke OB, Hamacher K, Colecraft HM, Mancia F, Hendrickson WA, Siegelbaum SA, DiFrancesco D, Bolognesi M, Thiel G, Santoro B & Moroni A. (2021). Gating movements and ion permeation in HCN4 pacemaker channels. *Mol Cell* **81,** 2929-2943.e2926.

Schulze-Bahr E, Neu A, Friederich P, Kaupp UB, Breithardt G, Pongs O & Isbrandt D. (2003). Pacemaker channel dysfunction in a patient with sinus node disease. *J Clin Invest* **111,** 1537-1545.

Schweizer PA, Duhme N, Thomas D, Becker R, Zehelein J, Draguhn A, Bruehl C, Katus HA & Koenen M. (2010). cAMP sensitivity of HCN pacemaker channels determines basal heart rate but is not critical for autonomic rate control. *Circ Arrhythm Electrophysiol* **3,** 542-552.

Schweizer PA, Schröter J, Greiner S, Haas J, Yampolsky P, Mereles D, Buss SJ, Seyler C, Bruehl C, Draguhn A, Koenen M, Meder B, Katus HA & Thomas D. (2014). The symptom complex of familial sinus node dysfunction and myocardial noncompaction is associated with mutations in the HCN4 channel. *J Am Coll Cardiol* **64,** 757-767.

Seifert R, Scholten A, Gauss R, Mincheva A, Lichter P & Kaupp UB. (1999). Molecular characterization of a slowly gating human hyperpolarization-activated channel predominantly expressed in thalamus, heart, and testis. *Proc Natl Acad Sci U S A* **96,** 9391-9396.

Seo H, Seol MJ & Lee K. (2015). Differential expression of hyperpolarization-activated cyclic nucleotide-gated channel subunits during hippocampal development in the mouse. *Mol Brain* **8,** 13.

Shi W, Wymore R, Yu H, Wu J, Wymore RT, Pan Z, Robinson RB, Dixon JE, McKinnon D & Cohen IS. (1999). Distribution and prevalence of hyperpolarization-activated cation channel (HCN) mRNA expression in cardiac tissues. *Circ Res* **85,** e1-6.

Shuster MJ, Camardo JS, Siegelbaum SA & Kandel ER. (1985). Cyclic AMP-dependent protein kinase closes the serotonin-sensitive K+ channels of Aplysia sensory neurones in cell-free membrane patches. *Nature* **313,** 392-395.

Stieber J, Stöckl G, Herrmann S, Hassfurth B & Hofmann F. (2005). Functional expression of the human HCN3 channel. *J Biol Chem* **280,** 34635-34643.

Ueda K, Nakamura K, Hayashi T, Inagaki N, Takahashi M, Arimura T, Morita H, Higashiuesato Y, Hirano Y, Yasunami M, Takishita S, Yamashina A, Ohe T, Sunamori M, Hiraoka M & Kimura A. (2004). Functional characterization of a trafficking-defective HCN4 mutation, D553N, associated with cardiac arrhythmia. *J Biol Chem* **279,** 27194-27198.

Velázquez Campoy A & Freire E. (2005). ITC in the post-genomic era...? Priceless. *Biophys Chem* **115,** 115-124.

Velázquez-Campoy A, Ohtaka H, Nezami A, Muzammil S & Freire E. (2004). Isothermal titration calorimetry. *Curr Protoc Cell Biol* **Chapter 17,** Unit 17.18.

Viscomi C, Altomare C, Bucchi A, Camatini E, Baruscotti M, Moroni A & DiFrancesco D. (2001). C terminus-mediated control of voltage and cAMP gating of hyperpolarization-activated cyclic nucleotide-gated channels. *J Biol Chem* **276,** 29930-29934.

Wainger BJ, DeGennaro M, Santoro B, Siegelbaum SA & Tibbs GR. (2001). Molecular mechanism of cAMP modulation of HCN pacemaker channels. *Nature* **411,** 805-810.

Wang J, Chen S & Siegelbaum SA. (2001). Regulation of hyperpolarization-activated HCN channel gating and cAMP modulation due to interactions of COOH terminus and core transmembrane regions. *J Gen Physiol* **118,** 237-250.

Weißgraeber S, Saponaro A, Thiel G & Hamacher K. (2017). A reduced mechanical model for cAMP-modulated gating in HCN channels. *Sci Rep* **7,** 40168.

Whitaker GM, Angoli D, Nazzari H, Shigemoto R & Accili EA. (2007). HCN2 and HCN4 isoforms self-assemble and co-assemble with equal preference to form functional pacemaker channels. *J Biol Chem* **282,** 22900-22909.

White DS, Chowdhury S, Idikuda V, Zhang R, Retterer ST, Goldsmith RH & Chanda B. (2021). cAMP binding to closed pacemaker ion channels is non-cooperative. *Nature* **595,** 606-610.

Wiseman T, Williston S, Brandts JF & Lin LN. (1989). Rapid measurement of binding constants and heats of binding using a new titration calorimeter. *Anal Biochem* **179,** 131-137.

Xu X, Marni F, Wu S, Su Z, Musayev F, Shrestha S, Xie C, Gao W, Liu Q & Zhou L. (2012). Local and global interpretations of a disease-causing mutation near the ligand entry path in hyperpolarization-activated cAMP-gated channel. *Structure* **20,** 2116-2123.

Xu X, Vysotskaya ZV, Liu Q & Zhou L. (2010). Structural basis for the cAMP-dependent gating in the human HCN4 channel. *J Biol Chem* **285,** 37082-37091.

Yanagihara K & Irisawa H. (1980). Inward current activated during hyperpolarization in the rabbit sinoatrial node cell. *Pflugers Arch* **385,** 11-19.

Yellen G. (1984). Relief of Na+ block of Ca2+-activated K+ channels by external cations. *J Gen Physiol* **84,** 187-199.

Zagotta WN, Olivier NB, Black KD, Young EC, Olson R & Gouaux E. (2003). Structural basis for modulation and agonist specificity of HCN pacemaker channels. *Nature* **425,** 200-205.

Zhou J, Ding WG, Makiyama T, Miyamoto A, Matsumoto Y, Kimura H, Tarutani Y, Zhao J, Wu J, Zang WJ, Matsuura H & Horie M. (2014). A novel HCN4 mutation, G1097W, is associated with atrioventricular block. *Circ J* **78,** 938-942.

Zhou L & Siegelbaum SA. (2007). Gating of HCN channels by cyclic nucleotides: residue contacts that underlie ligand binding, selectivity, and efficacy. *Structure* **15,** 655-670.

Appendix

Schematic diagram of the protein used in the thesis

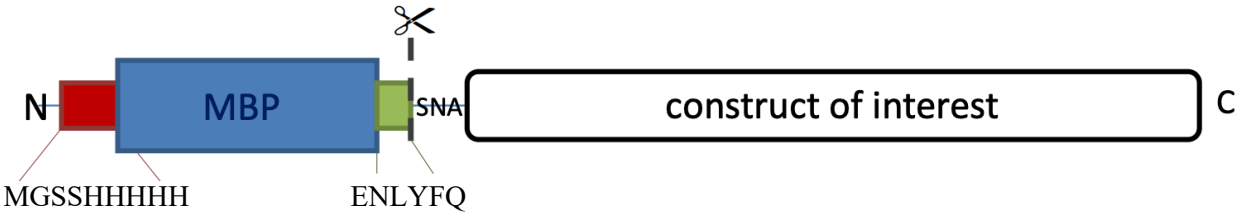

HCN4 (Oryctolagus cuniulus) i. 522-725

DSSRRQYQEKYKQVEQYMSFHKLPPDTRQRIHDYYEHRYQGKMFDEESILGELSEPLRE

EIINFNCRKLVASMPLFANADPNFVTSMLTKLRFEVFQPGDYIIREGTIGKKMYFIQHGV

VSVLTKGNKETKLADGSYFGEICLLTRGRRTASVRADTYCRLYSLSVDNFNEVLEEYPM

MRRAFETVALDRLDRIGKKNSILLHK

Sets of forward and reverse primer for performing R524Q site-directed mutagenesis in HCN4

5’-GCAGATTCGTCA**CAG**CGCCAATACCAG-3’

5’-CGTCTAAGCAGT**GTC**GCGGTTATGGTC-3’

Set of forward and reverse primer for performing R550C site-directed mutagenesis in HCN4

5’ - GACACCCGCCAGTGCATCCACGACTAC -3’

3’ - CTGTGGGCGGTCACGTAGGTGCTGATG -5’